FINITE ELEMENT MODELING OF GLASS FIBER REINFORCED PLASTIC PIPES UNDER IMPACT LOADING

BY

RUBAIAN FAHED AL-SHAHRANI

A Thesis Presented to the

DEANSHIP OF GRADUATE STUDIES

KING FAHD UNIVERSITY OF PETROLEUM & MINERALS

DHAHRAN, SAUDI ARABIA

In Partial Fulfillment of the
Requirements for the Degree of

MASTER OF SCIENCE

In

MECHANICAL ENGINEERING

DECEMBER 2013

KING FAHD UNIVERSITY OF PETROLEUM & MINERALS
DHAHRAN- 31261, SAUDI ARABIA
DEANSHIP OF GRADUATE STUDIES

This thesis, written by RUBAIAN FAHED AL-SHAHRANI under the direction his thesis advisor and approved by his thesis committee, has been presented and accepted by the Dean of Graduate Studies, in partial fulfillment of the requirements for the degree of **MASTER OF SCIENCE IN MECHANICAL ENGINEERING.**

Thesis Committee

Dr. Nesar Merah
(Advisor)

Dr. Yagoub N. Al-Nassar
(Member)

Dr. Shafique Khan
(Member)

Dr. Zuhair M. Gasem
Department Chairman

Dr. Salam A. Zummo
Dean of Graduate Studies

25/12/13
Date

DEDICATION

Special thanks for my parents and family who lived with me every single moment of this journey. Their passion, dedication and perseverance support had driven me to exert the utmost effort I can do to achieve this goal and be awarded with M.Sc. in Mechanical Engineering.

ACKNOWLEDGMENTS

All praise to Allah for his endless graces that The Almighty awards us during our entire life. Completing this work was happen because of his support and providing the needed help along this journey. Acknowledgment is due to the King Fahd University of Petroleum & Minerals for supporting this research.

I am pleased to express my sincere gratitude to Dr. Nesar Merah who served as my major advisor. I also express my deep thankfulness to the other members of my thesis committee Dr. Yagoub N. Al-Nassar and Dr. Shafique Khan. The tremendous effort they exerted is really highly appreciated. The guidance, inspiration and support provided by my thesis advisor played a major role in achieving this accomplishment. Working with my thesis committee members was a great learning opportunity.

I would like to thank all individuals who provided me support and help during my study.

TABLE OF CONTENTS

LIST OF TABLES

LIST OF FIGURES

THESIS ABSTRACT

NAME: **RUBAIAN FAHED ABDULRAHMAN AL-SHAHRANI**

TITLE: **FINITE ELEMENT MODELING OF GLASS FIBER REINFORCED PLASTIC PIPES UNDER IMPACT LOADING**

MAJOR: **MECHANICAL ENGINEERING**

DATE: **DECEMBER, 2013**

Due to properties such as good corrosion resistance, durability and high strength-to-weight ratio, Glass-Fiber Reinforced Epoxy (GFRE) pipes are finding increasing use in water, crude oil and other chemicals' handling and transportation. However, the high mechanical performance of GFRE pipes and structures may be adversely affected by their low resistance to impact loadings. The low-velocity impact loads are particularly more dangerous as their damage to the structural integrity of the composite pipes often goes undetected.

In the present work, the behavior of GFRE pipes under low-velocity impact loads are modeled using finite element analysis. Four-node quadrilateral layered shell elements are selected to model the filament wound GFRE pipe with eight (8) layers oriented at 54.5º & -54.5º which is simply supported. The solid steel cylindrical impactor with a hemispherical tip is modeled using 8-node brick elements. Incident impact energies in the range of 12 to 110 J were considered in the analysis. The load-time traces of the GFRE pipes under these impact energies show good agreement with published numerical and experimental results. The model was then used to predict the composite structure failure under 12 J, 35 J, 80 J and 110 J resulting in damage initiation at lower energies (12 J & 35 J) and penetration at higher energies (80 J and 110 J) for GFRE pipes with wall thicknesses of 4.5 mm and 6 mm. Under similar conditions and range of impact energy, the damage through 4.5 mm wall thickness was found to be more severe than for 6 mm wall thickness pipes.

MASTER OF SCIENCE DEGREE

KING FAHD UNIVERSITY OF PETROLEUM & MINERALS

Dhahran, Saudi Arabia

THESIS ABSTRACT (ARABIC)
ملخص الرسالة

الاســــــــــم: **ربيعان فاهد عبدالرحمن الشهراني**

عنوان الرسالة: **محاكاة العناصر المحددة لأنابيب الألياف الزجاجية المقواة بالبلاستيك تحت تأثير قوى الاصطدام**

التخصـــــــص: **الهندسة الميكانيكية**

تاريخ التخـرج: **ديسمبر / 2013**

نظرا لخصائص أنابيب الألياف الزجاجية المقواة بالبلاستيك مثل المقاومة الجيدة للتآكل، وقوة التحمل، وارتفاع نسبة القوة إلى الوزن، أصبحت أكثر استخداما في نقل المياه، والنفط الخام، والمواد الكيميائية الأخرى والتعامل معها. ومع ذلك، فإن ميكانيكية الأداء العالية لأنابيب وهياكل لألياف الزجاجية المقواة بالبلاستيك قد تتأثر سلبا بسبب انخفاض مقاومتها لقوى الاصطدام. إن تأثير قوى الاصطدام المنخفضة السرعة بشكل خاص يعتبر أكثر خطورة وذلك لصعوبة اكتشاف الأضرار الناتجة عنها في الغالب والتي تؤثر في سلامة البنية التركيبية للأنابيب.
في هذه الدراسة، يتم محاكاة سلوك أنابيب الألياف الزجاجية المقواة بالبلاستيك تحت تأثير قوى الاصطدام المنخفضة السرعة باستخدام تحليل العناصر المحددة. وقد تم بناء نموذج الاختبار باختيار عناصر رباعية الأطراف ذات طبقات اسطوانية الشكل لمحاكاة بناء الأنابيب والمكونة من ثمان طبقات مثبتة فوق بعضها البعض بزاويتي الاتجاه 54.5 و -54.5 درجة وبشكل متسلسل، ووضع الأنبوب أفقيا بشكل مبسط على قوائم مثبته على أرضية أفقية. كما تم بناء نموذجا لقذيفة اسطوانية من الفولاذ ذات نهاية نصف كروية من مادة صلبة مكونة من عناصر ثمانية الأطراف. وقد أخذ بالاعتبار طاقات الاصطدام من 12 إلى 110 جول بهدف تحليل الأثر الناتج.
وقد أظهرت نتائج قوى الاصطدام بالنسبة للوقت لأنابيب الألياف الزجاجية المقواة بالبلاستيك تحت تأثير طاقات الاصطدام هذه توافقا جيدا مع نتائج نماذج المحاكاة والتجارب العملية المنشورة. وبعد ذلك تم استخدام هذا النموذج للتنبؤ بحدوث الضرر لبنية المادة التركيبية تحت تأثير 12 و 35 و 80 و 110 جول، مما نتج عنه بداية للتلف عند طاقات الاصطدام الدنيا (12 و 35 جول) والاختراق عند طاقات الاصطدام العليا (80 و 110 جول) لأنابيب لألياف الزجاجية المقواة بالبلاستيك ذات السمك 4.5 ملم و 6 ملم، على التوالي. وفي ظل ظروف مماثلة، وتحت تأثير مجموعة مشابهه من طاقات الاصطدام، ثم استنتاج أن الضرر الحاصل لأنابيب لألياف الزجاجية المقواة بالبلاستيك ذات السمك 4.5 ملم كان أكثر شدة من الأنابيب ذات السمك 6 ملم.

درجة الماجستير في العلوم

جامعة الملك فهد للبترول والمعادن

الظهران - المملكة العربية السعودية

CHAPTER 1

INTRODUCTION

Because of their good corrosion resistance, durability and high strength-to-weight ratio, the use of the Glass-Fiber Reinforced Epoxy (GFRE) pipes has increased in many diverse industries such as, off-shore marine, chemical processing and pressure piping. However, these materials are susceptible to have degradation of their mechanical performance, reduction of structural integrity and fluid leakage due to incidental low velocity impacts, either in service or during handling. Low-velocity impacts can produce local indentation and delamination which are often difficult to detect. This shows the need for full characterization of GFRE pipes behavior under dynamic loading conditions by assessing the extent of such failures and how they affect the pipes' mechanical properties.

1.1 Composite Materials

Composite materials are constituted of two or more materials with significantly different mechanical properties to obtain a new material with high mechanical performance. These two constituent materials are known as matrix and reinforcement. The type of matrix such as polymer, metallic and ceramic is the common base that composites are normally

classified in. In fiber–reinforced composites, fibers are the principal load carrying members, while the surrounding matrix keeps them in the desired location and orientation. The matrix also acts as a load transfer medium between the fibers and protects them from environmental damages due to elevated temperatures, humidity and corrosion. The principal fibers in commercial use are various types of glass, carbon and aramid [1, 2].

1.2 Glass Fiber Reinforced Epoxy (GFRE)

GFRE pipes have been proven to have an excellent ability to transport corrosive liquids due to their superior corrosion resistance and low coefficient of friction. Many studies were conducted to investigate the suitability of thermosetting-based resin pipes with glass fiber reinforcement for different industry applications, including but not limited to, water storage tanks, desalination, chemical, and oil and gas industries.

1.2.1 Fiber Reinforcement

The fiber is used as reinforcement in composites. The fiber generally occupies 30%-70% of the matrix volume in the composites [1, 2]. The fibers can be chopped, woven, stitched, and/or braided. They are usually treated with sizing such as starch, gelatin, oil or wax to improve the bond as well as binders to improve the handling. The most common types of fibers used in advanced composites for structural applications are the glass, aramid, and carbon. The glass fibers are the least expensive and carbon fibers being the most expensive. The cost of aramid fibers is about the same as the lower grades of the

carbon fiber. Other high strength high-modulus fibers such as boron are at the present time considered to be economically prohibitive [1, 2].

1.2.2 Glass Fibers

Glass fibers are the most widely used reinforcement material due to its low cost, high tensile and impact strength, light weight and good corrosion resistance. Hence, epoxy and vinyl ester resins reinforced with glass fibers represent potential composite materials for the oil and gas industry.

Glass fiber reinforcements are classified based on their properties. There are five major types of glass used to make fibers which are [3]:

1. A-glass is a high-alkali glass containing 25% soda and lime. It offers very good resistance to chemicals but lower electrical properties.

2. C-glass is chemical glass which works with extremely high chemical resistance.

3. E-glass is electrical grade with low alkali content. It has better electrical insulation and strong resistance from water attack. E-glass represents more than 50% of the glass fibers used for reinforcement.

4. S-glass is a high-strength glass. It is 33% higher tensile strength than E-glass.

5. D-glass has superior electrical properties but not mechanically as good as E- or S-glass.

1.2.3 Polymer Matrix

A polymer matrix material or resin solution is considered the other constituent in composites. There are two classes of resins: thermoplastics and thermosets. Unlike thermoplastics, thermosets are suitable for structural application because of their ability to permanently cure. Polyester, vinyl ester, epoxy, phenolic, and polyimide are the most common categories of thermosets. Thermosets as matrix material are used to transfer stresses between fibers to provide an adverse environment and protect the surface of the fibers from mechanical abrasion. The matrix plays a major role in the inter-laminar and in-plane shear load transfer.

1.3 Need for Finite Element Analysis

The need for Finite Element Analysis (FEA) stems from the necessity for a predictive analysis of impact loading events. Several investigations were performed to examine the impact loading of fiber reinforced composites materials using finite element method (FEM) [4]. Some previous studies reported the use of the 2D FE beam-like model which is computationally very efficient due to its simplicity and its ability to study some fundamental impact cases. However, there is a limitation of this model to provide more detailed for damage such as the in-plane delamination shape in the laminated plates for plane-strain problems. 3D FE models were used to analyze the stress in the laminates with more details. The excessive computational cost and the challenges while producing automatic mesh generation with the extension of delamination have considered as part of

difficulties that limit the use of 3D FE models. Therefore, some researchers applied the 2D plate model to cope such challenges [5].

Using FEM can help understand the impact damage process more comprehensively. Researchers found that this numerical model can capture the main features of impact phenomenon and reasonably predict various damage modes [6].

1.4 Finite Element Techniques

In general, the implicit and explicit methods are the two FE solution techniques that are used in commercial FE software packages. For linear and moderate non-linear problems, the implicit method is used while the explicit method is successfully used for highly non-linear problems and dynamic analysis such as composites' impact analysis. The dynamic formulation can easily control the instability of geometry and material softening occurring during the simulation [7].

1.5 Present Study

The main objective of this thesis work is to develop and validate a FE model of a GFRE pipe for applications in water and crude oil transportation and handling and use the model to quantify the damage caused by low velocity impact loading. The modeling of the problem and the damage evaluation are accomplished using ANSYS/LS-DYNA commercial packages.

The thesis is divided into five chapters. Chapter 1 presents the introduction of the study which includes basic information regarding composites and their properties, glass fibers and polymer matrix. Chapter 2 covers the literature review that summarizes previous relevant research work on the experimental impact testing and related numerical analyses of the composite materials. The development of the FE model along with the details of examined GFRE pipes are provided in Chapter 3. The results for modeling and damage evaluation of the GFRE composite pipes are presented and discussed in Chapter 4. Finally, conclusions drawn from this study and recommendations for future work are provided in Chapter 5.

CHAPTER 2

LITERATURE REVIEW

The present chapter will focus on reviewing experimental and numerical research work related to the impact resistance of GFRE materials.

2.1 Experimental Investigation of GFRE Behavior under Impact Loading

Naik et al. [1] and Khan et al. [2] studied the effect of environmental degradation on the performance and durability of the GFRE pipes using several mechanical tests including tensile, fatigue, creep, flexural, fracture toughness, hydro-burst pressure and low velocity impact tests. The specimen were made of vinyl ester based (GFRV) and epoxy based (GFRE) filament wound glass fiber reinforced thermoset pipes of 8 plies with a ply angle of ±54.5º. The pipes had dimensions of 150 mm internal diameter and 6 mm thickness. The authors [1, 2] found that there was about 80% reduction in the pipes pressure performance for high energy impact.

Alderson and Evans [8] conducted static and low velocity (up to 10 m/s) impact tests using 36 Kg tup on GFR filament-wound pipes with two different support conditions

involving floor supported and end simply supported. The tested pipes were made of E-glass/Epoxy resin with a ply angle of ±55º and glass volume fraction of 56%. The specimens had dimensions of 162 mm external diameter, 6 mm thick and 500 mm long. The authors found that the tested specimens endured a two-part failure process; (1) Delamination initiation and local crushing occurred at the end of elastic behavior at the approximate same load regardless of support condition. A drop in load was observed at this point. (2) The subsequent delaminations continued with a concomitant increase in load until a second major failure, which is the fast-rated delaminations growth, occurred first for the simply supported pipes and then for the floor supported pipes at higher loads. The test results showed an agreement between static and impact tests. Moreover, the impact damage was found to be similar, with high severity, to static damage but the pipe was still capable of carrying more load.

Gning et al. [9] studied experimentally the damage development in thick filament-wound E-glass/Epoxy pipe of 110 mm long, 55 mm internal diameter and 6 mm thick at different levels of energy (up to 45 J) with both static and impact loading. The pipes were made of 20 plies with a ply angle of ±55º and fiber volume fraction of 62%. At low impact energy, a small local indentation occurred at the contact area of the upper layers of about 0.3 mm thickness. Then, the damage initiation started at the threshold energy level in the form of delamination which propagated through the pipe thickness. The transverse intra-layer cracks appeared for higher impact energy. Load-displacement plots showed an increase in contact duration and projectile displacement (i.e. the displacement of impactor tip into the pipe during the impact event) as projectile velocity and impact energy elevated. The dimensions of the damage in the axial and circumferential directions on the

upper side of the pipe were found much closer to circular shape for low energy while the damage zone expanded for higher impact energy and took the square shape.

Ruhala and Engel [10] studied the behavior of E-glass/Epoxy composite plates under low velocity impact loading and how relative fiber contents affect the impact properties. The hand lay-up method was used to fabricate the plates in a stacking sequence of $[0/90/0/\overline{90}]_s$ for different fiber volume fractions of 40, 60 and 80. The fiber weight percents and densities are the properties that were utilized to control the differences in relative fiber contents of the plates. The authors found that, by increasing the relative amount of fiber weight of the plate and decreasing the density, the fiber volume fractions did not increase due to the increase of voids with the relative fiber content. The associated damage with the impact events started with an elastic deformation while the load was increased until the permanent deformation occurred in forms of matrix cracking and delaminations. A slight drop in the load was observed at this point then the force-time curve began to rise again. When the force reached the maximum, fiber breakage occurred and unstable matrix crack and delaminations took place. As the load drops off, some cracks and delaminations were observed as the tup passed through the plate. Similar failure modes have been identified by Alderson and Evans [8]. In penetration case, the damage absorbed a large amount of impact energy while for non-penetrated plates, there was some stored energy that allowed the plate to cause rebounding of the tup.

Belingardi and Vadori [11] examined the behavior of GFRE composite laminate plates subjected to low velocity impact loading. The tested specimens were made of glass/epoxy composite plates in three different cross-ply configurations of$[0/90]_s$, $[0/+60/$

$-60]_s$ and $[0/+40/-40]_s$ with unidirectional and woven layout. The fiber weight percents varied between 62 and 66% while the plates' thickness and density stayed the same at 2 mm and 1.99 kg/dm^3, respectively. The study identified two thresholds: the first material damage force where the force oscillations took place and the maximum force where the material can carry the maximum load capacity. Alderson and Evans [8] and Ruhala and Engel [10] reported similar results. The examined energy results supported defining two energy absorption parameters, namely: the saturation impact energy (the maximum energy that the material can stand for without perforation) and the damage degree (the ratio of dissipated energy to the total transformed energy during the impact).

2.2 Finite Element Analysis

Okoli and Abdul-Latif [4] conducted a study to determine the relationship between the experimental and predicted data of the impact behavior of a cross-ply plain weave $[0/90]$ glass/epoxy composite laminate. The specimens' dimensions were 200 mm long, 15 mm wide and 3 mm thick with 18 layers and glass volume fraction of 70%. The data used in the DYNA3D were obtained by extrapolating results from the low to intermediate rate tensile tests. The findings suggested that a predictive analysis is more accurate at a speed of2 m s^{-1} than at 4 m s^{-1} analysis. Therefore, the accuracy of the FEM decreases with an increase in impact velocity. It was reported that there is a considerable difference of the final velocity between FEM and the test results. This indicated that the

laminate fracture dissipated energy is less in the FEM compared to the experimental test. The study concluded that the extrapolation of data is a valid method for obtaining data at high strain rates into a numerical simulation.

Li et al. [5,6] developed a numerical model to investigate the process of low-velocity impact damage of cross-ply fiber-reinforced carbon/epoxy composite laminates using the FEM. The tested plates had the stacking sequence of $[(0/90/0]$. The authors used an integrated numerical model with 9-node Lagrangian plate element to illustrate different type of damages including fiber breakage, matrix cracking and delamination and their associated influences. Also, within this model, various aspects for instance the impact failure criteria, plate stiffness update, dynamic contact problem between delaminated layers and computational efficiency improvement through the adaptive analyses were studied in detail. The adaptive analyses included the time increment adjustment, the stiffness matrix update with respect to the current extent of deformation and penalty parameters modification followed current caused damage. The authors investigated the effects of various parameters on the impact process, especially on the impact-induced damages, including the size of target plate, the boundary conditions, the impactor mass and impact velocity using FEM. The authors found that this numerical model was able to simulate the main features of impact process and predict various damages and the following conclusions had been reached:

a. The plate size influence was not noticeable on the size of delamination unless the impact velocity was high. On the other hand, increasing the size of plate led to an

increase in the maximum central deflection and a decrease in the maximum impact force

b. The impactor mass significantly affected the impact process. The maximum impact force increased when the impactor mass decreased and impact velocity increased. Subsequently, matrix cracks area and size of delamination increased.

Elder et al. [12] provided a state of art review for predicting delamination of laminated composites under low velocity impact to improve the numerical simulation methodology that can better predict the delamination. The linear elastic fracture mechanics (LEFM) is the common applied method for predicting the inter-ply delamination front shape and can provide reasonably accepted shape mesh. However, LEFM was found not to be the most appropriate method to predict the irregular shaped delamination fronts occurring during the impact phenomenon. The boundary element (BE) method was used to analyze 3-D crack propagation. The significant limitation of BE method to find a fundamental solution for the material that is stressed beyond its elastic limit was overcome by including material plasticity and cohesive fracture within this method. The authors found that the cohesive fracture model can overcome some of the limitation of the LEFM method. It can be considered for layered shell and solid elements. They concluded that the delamination threshold load method is a simple methodology to predict delamination and provide good results.

Naik and Meduri [13] studied the impact behavior of simply supported polymer-matrix composite plates subjected to low velocity impact load. The plates were made of E-glass/Epoxy composite in dimensions of 150 mm x 50 mm x 6 mm with fiber volume

fraction of 0.4 and density of 1750 kg/dm^3. Prediction of in-plane failure of layers in the form of matrix cracking and delaminations had been investigated. 3D transient finite-element analysis with quadratic failure criteria had been used to predict in-plane and interlaminar failure initiation. The authors observed that mixing of unidirectional and woven-fabric layers results in increased impact damage resistance.

Gning et al. [14] performed a study to identify and model the damage initiation and damage tolerance development in glass-reinforced epoxy composite filament-wound pipes subjected to drop weight impact. The examined pipes were made of E-glass/Epoxy resin with stacking sequence of $[\pm 55°]_{10}$ and glass volume fraction of 61%. Models had been developed using ABAQUS to simulate the dynamic response of the above specified pipes then the damage criteria were applied to analyze these models. It has been shown that the impact damage reduced the residual implosion strength of glass/epoxy cylinders significantly. A 12-J impact reduced the implosion pressure by 40%. Naik et al. [1] reported about 80% reduction in the pipes performance pressure at 35 J and above.

Aslan et al. [15] studied experimentally the low-velocity impact of cross-ply E-glass/Epoxy laminated composite plates consisting of $(0/90/0/90)_s$ lay-up configuration. The tests were conducted on three plates in dimensions of 150-mm x 150-mm x 4.8-mm, 150-mm x 100-mm x 4.8-mm and 150-mm x 50-mm x 4.8-mm with fiber volume fraction of 57%. The transient dynamic FE 3DIMPACT code was used in developing a numerical model in order to determine the impact load and stresses of the plates beside a failure analysis of the caused damage. The authors found that there was a remarkable variation in the load-time curves as the impactor mass changed. In contrast

with the experimental results, the numerically predicted values for impact force were found higher along with shorter period of contact period. The in-plane dimensions had an influence on the composite structures' mechanical behavior where the contact duration increased with the decrease of the plate width dimension.

Yen et al. [16] developed progressive failure criteria for impact analysis of composite structures that covered fiber failure, matrix failure and delamination. They used an explicit dynamic FE code to determine the nonlinear behavior of the composite cylindrical shapes subjected to drop weight impact loading. The authors examined a Graphite/Epoxy composite laminate pipe consisting of 8 layers with the stacking sequence of [30/-30/90/90/30/-30/90/90] and having dimensions of 150-mm internal diameter, 6-mm thickness and 300-mm length under impact conditions to predict the load-time history and damage using the 4-node shell elements in LS-DYNA code. In conclusion, results showed good correlation with the experimental data.

Kim et al. [17] developed a 3D FE model to describe the dynamic behavior and impact induced damage of shell composite structures using 8-node brick elements with Taylor's modifications. The numerical analysis was carried out on the carbon-fiber-reinforced plastic (CFRP) cylindrical shells with a curvature radius of 50 mm and three different cross-ply configurations: $[0/90/0/90/]_4$, $[90/0/90/0/]_4$ and $[45/-45/45/-45/]_4$. Hashin's criterion was used to predict the matrix cracking and semi-empirical criterion for delamination. The impact force was calculated by using the modified Hertzian contact law and found that it became higher as the shell curvature increased. The authors found also that the area of delamination in shells was wider than in plates under the same

applied conditions. The progressive failure through the composite thickness was reported to be different in plate and shell composite structures.

Zhao and Cho [18] investigated the initiation of impact induced damage and its propagation in composite shell subjected to drop weight impact. The distribution of the interlaminar stress and damage propagation had been analyzed using 8-node element with Taylor's modification scheme. Their analysis scheme was similar to that of Kim et al. [17] . The failure modes of matrix cracking, fiber breakage and delamiantion had been investigated. The authors reported that using Tasi-Wu quadratic failure criterion was not recommended since the damage modes cannot be differentiated by this criterion, therefore, additional criteria including Tsai's damage modes delamination formula were applied at all Gaussian points. The initial matrix damage was caused by the interlaminar shear stress and in-plane transverse stress while out-of-plane normal tensile and shear stresses were important for causing delamination. The damage through propagation was found to behave differently in composite shell and plate. In case of shell, the outer layers got damaged first then progressively followed by inner layers but it was opposite situation in the case of plate.

Hosseinzadeh et al. [19] studied experimentally the behavior of fiber reinforced composite plates subjected to drop weight impact loading. The test was performed on four types of fiber reinforced composites including thin/thick Glass Woven/Epoxy (GFRE) plates, Carbon/Epoxy (CFRE) plate and Carbon/Glass Woven/Epoxy (CGFRE) plate under four impact energies ranging from 30 to 100J. The results showed that the behavior of CFRE plates under low velocity impacts was the best and CGFRE plates had

suitable behavior under high impact energy. Numerical models for the tested plates were generated using ANSYS/LS-DYNA software. The FE code results showed a good correlation with experimental data in predicting the threshold of damage but no coincidence with similar damage shape in the post-failure behavior.

Her and Liang [20] examined the composite laminate and shell structures subjected to low velocity impact using the ANSYS/LS-DYNA FE code. The modified Hertz contact law was used to calculate the contact force. A model of Graphite/Epoxy composite laminate shell structures consisting of stacking sequence of [0/90/0/90/0] and thickness of 2.54 mm was developed for both cylindrical and spherical shells. The study covered the effects of shell curvature, clamped or simple support boundary conditions and impactor velocity. The results showed good correlation with the literature. The authors found that with smaller curvature and clamped boundary conditions resulted into larger impact force and smaller deflection. They also reported a proportional relation between the impact response and the impactor velocity.

2.3 Summary of Literature Review

There was a focus through this review on the experimental and numerical investigations that studied the effect of low velocity impact loading on fiber reinforced composite glass/epoxy structures, in particular. Several studies have been devoted to understanding the mechanisms and mechanics of the impact loading damage in the composite laminate structures and building up clear relationship between various parameters of impact events

and those of damage extents. The impact process and associated damage failures started with a small local indentation occurring at the contact area of the upper layers at low impact energy. Then, the damage initiation started at the threshold energy level in the form of delamination which propagated through the pipe/shell thickness. The transverse intra-layer cracks appeared for higher impact energy. Some simple empirical formulae or simplified models with the aid of experimental information have been used in some of the numerical approaches to roughly evaluate the delamination size while some others made the assumption that the low velocity impact being simulated was essentially a quasi-static event and hence used implicit solvers. In an explicit dynamic analysis code, failure models are integrated into the load step/time regime to determine the nonlinear behavior of the composite structures subjected to drop weight impact loading. Using the explicit method in impact investigation helps to simulate the main features of impact process and predict various damages that were found capable for analyzing dynamic, highly non-linear problems, particularly where contact plays an important role.

2.4 Motivation for Present Investigation

As discussed above, organic matrix fiber reinforced composite laminates are very susceptible to low-velocity transverse impact which could cause matrix cracks, delamination and fiber breakage in fiber-reinforced polymer composite laminates. Such damages, especially delaminations, can cause significant reductions in the compressive strength of laminates and influence the reliability of structures. GFRE pipes when impacted suffer damage which causes a reduction in their ability to withstand internal

pressure leading to leakage of liquid. Understanding and quantifying this damage is of utmost importance to the designers. This quantification by numerical methods such as FEM requires precise modeling of the impact event and material behavior under this type of load. The modeling of dynamic impact loading of GFRE pipe is a complex exercise. The present work undertakes at performing the modeling and analysis of the GFRE pipes under low velocity impact loading.

2.5 Objective of the Present Study

The main objective of this thesis work is to develop a proper FE model of filament wound GFRE pipe destined for water and crude oil transportation and handling under low-velocity dynamic impact. The model is then used to predict the behavior of the structure of the pipe under different impact energies ranging from 12 to 110J using ANSYS program combined with LS-DYNA features. The numerical results will be validated with the existing numerical and experimental results obtained under similar conditions.

The specific objectives of this work are as follows:

1. Develop a FE model for a filament wound GFRE pipe and impactor.
2. Validate numerical output involving force vs. time with existing numerical and experimental results.

3. Use the results to quantify damage under different impact energies ranging from 12 to110 J.

4. Perform FE model for a filament wound GFRE pipe with different wall thicknesses and determine the effect of thickness on the impact resistance of the GFRE pipes.

The results of this work may serve as the basis for additional research to optimize the GFRE pipes manufacturing processes and deploy their application in new areas such as oil and gas industry. These objectives will be fulfilled in the next chapters.

CHAPTER 3

FINITE ELEMENT MODEL

3.1 Development of Finite Element Model

Composites, as anisotropic materials, are considered to be more challenging to model than isotropic materials such as aluminum and steel. Each layer in a composite laminate may have different orthotropic material properties, therefore, the properties and orientations of the various layers should be defined with special care. ANSYS allows modeling of composite materials with specialized elements called layered elements. The modeling process of a section of a GFRE pipe under drop weight impact is explained in the following section.

3.1.1 Development of Geometrical Model

Low velocity impact modeling is carried out using a hemispherical impactor with 12.7 mm diameter spherical head and a rigid body of 50 mm diameter and 66 mm length. The mass of drop weight will be taken as 10 kg for low impact energy while 25 kg will be considered for higher impact energy. The GFRE pipe is 300 mm long with 150 mm internal diameter and 6 mm thickness, as shown in Fig. 3.1. These dimensions and loading conditions are selected to conform with the experimental tests performed by Naik et al. [1], Khan et al. [2] and according to ASTM D2444-99 and ASTM D2290-08 [21,

22]. The pipe has been considered as a thin cylinder given that its thickness is less than $1/20^{th}$ of the diameter as shown below:

$$\frac{\text{Thickness}}{\text{Diameter}} = \frac{6}{162} = 0.037 \text{ mm} < \frac{1}{20}$$

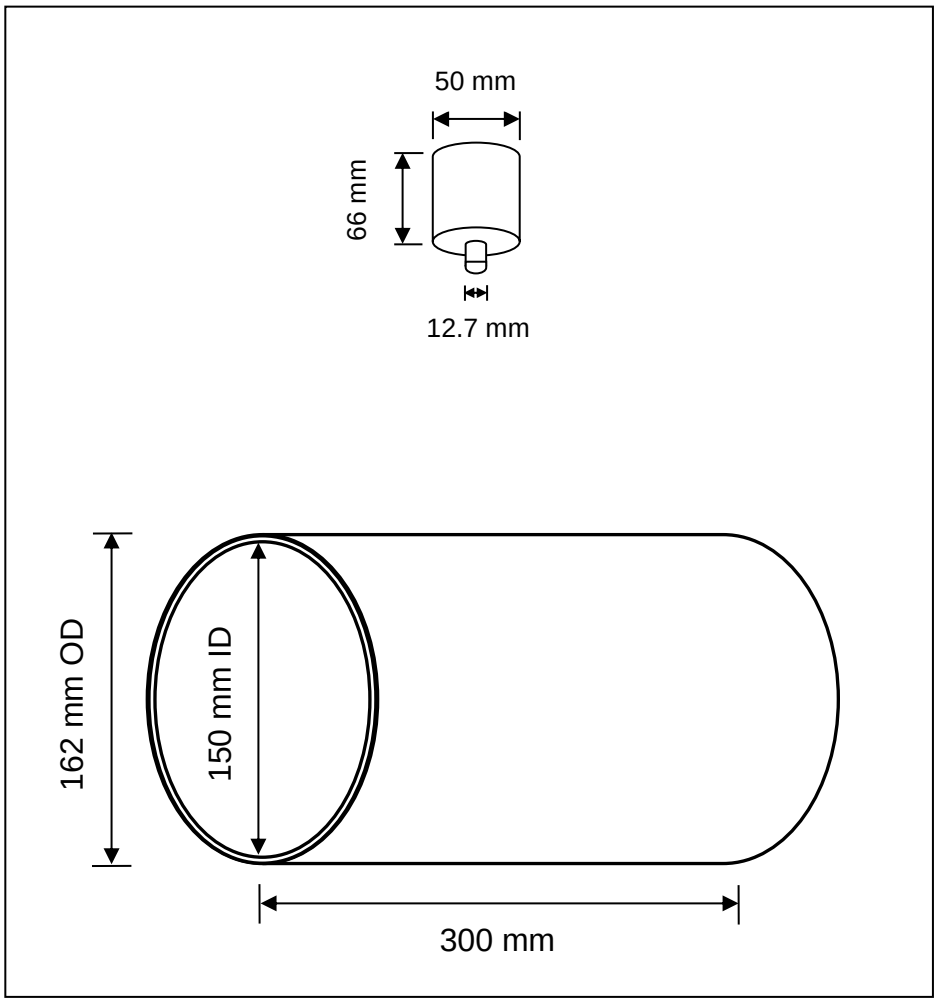

Figure 3.1 Geometry of GFRE pipe and rigid body impactor

3.1.2 Meshing

A full section of pipe was modeled due to the inherent nonsymmetrical nature of the geometry of laminate with a ply angle of ±54.5º. In this work, the discretization process is performed by subdividing the pipe into distinct finite elements as shown in Fig. 3.2. To get more accurate results, a fine grid size has been applied in the regions located near the impact center (i.e. high deformation region) while gradually large grid sizes were used away from impact area as shown in Fig. 3.3. When choosing the mesh type, the set-up time and the computational expenses were considered.

Analyzing different mesh scales was required to decide what will be the appropriate mesh density until two meshes gave nearly the same results, then the mesh was considered adequate and used in the analysis.

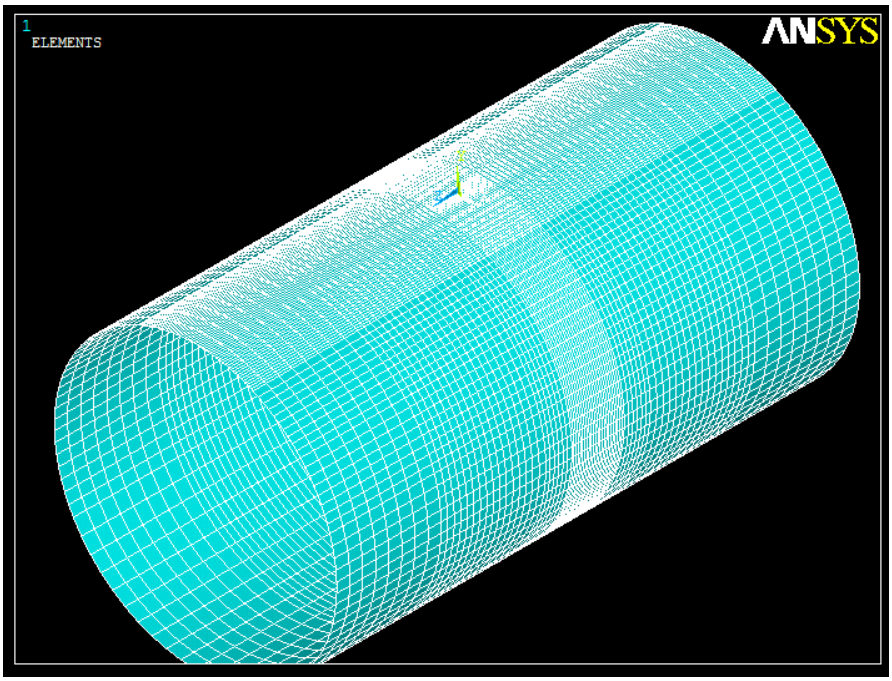

Figure 3.2 Refined finite element mesh for GFRE pipe section

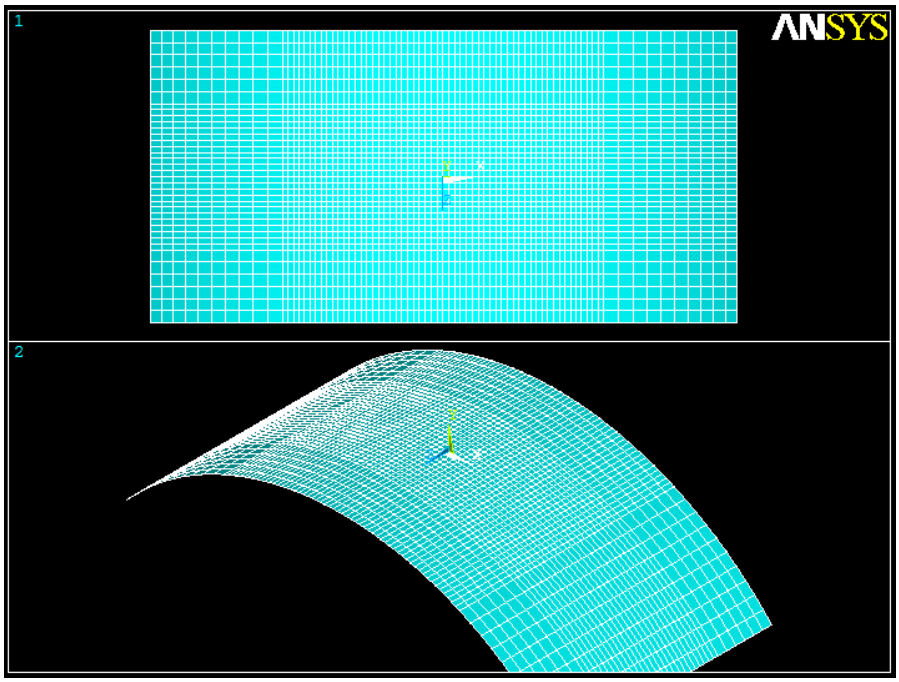

Figure 3.3 Refined finite element mesh for GFRE pipe impact cross-section

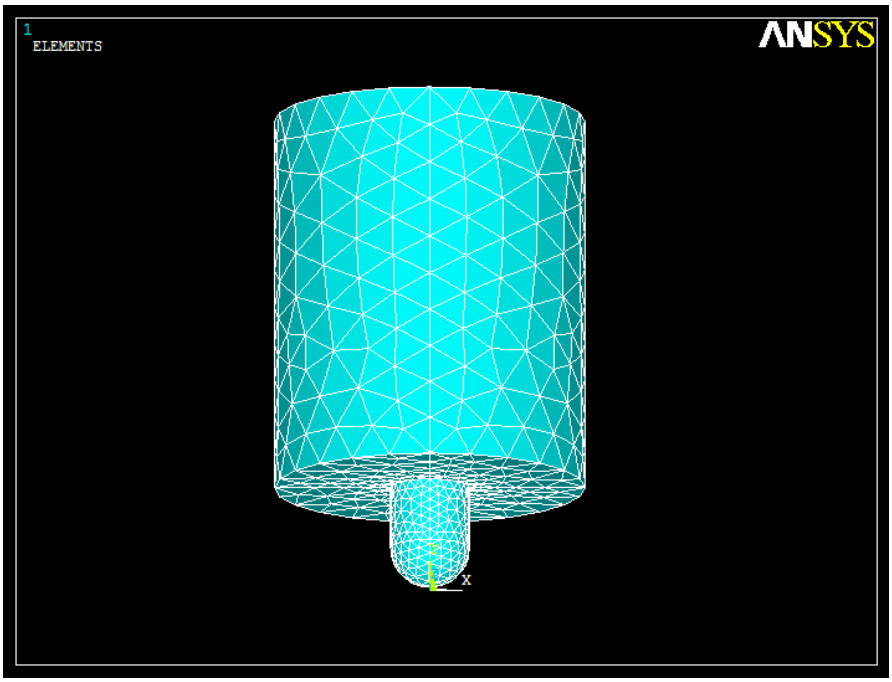

Figure 3.4 Finite Element mesh for steel impactor

a) Types of Elements

The present GFRE pipe material is an orthotropic elastic type, therefore, it is recommended that a 4-node quadrilateral layered shell element shown in Fig. 3.5 be used in the model [16]. For a multi-layer composite laminate, the "TB,COMP" command is used as a designated activation in data table for nonlinear material properties and the lamina (ply) properties are specified as SHELL163 real constants [23]. Each node has twelve degrees of freedom (DOFs) including translations (Ux, Uy, Uz), velocities (Vx, Vy, Vz) and accelerations (Ax, Ay, Az) in the nodal X, Y, and Z directions, in addition to rotations (Rotx, Roty, Rotz) about the nodal X, Y, and Z axes, respectively. It is

important to note that velocities (Vx, Vy, Vz) and accelerations (Ax, Ay, Az) appear as DOFs while they are not actually physical DOFs. However, these quantities are computed as DOF solutions and stored for post processing. That leads to confirm that 4-node SHELL element actually has only six DOFs. Unlike most implicit analyses, all loads in an explicit analysis must be time-dependent in nature.

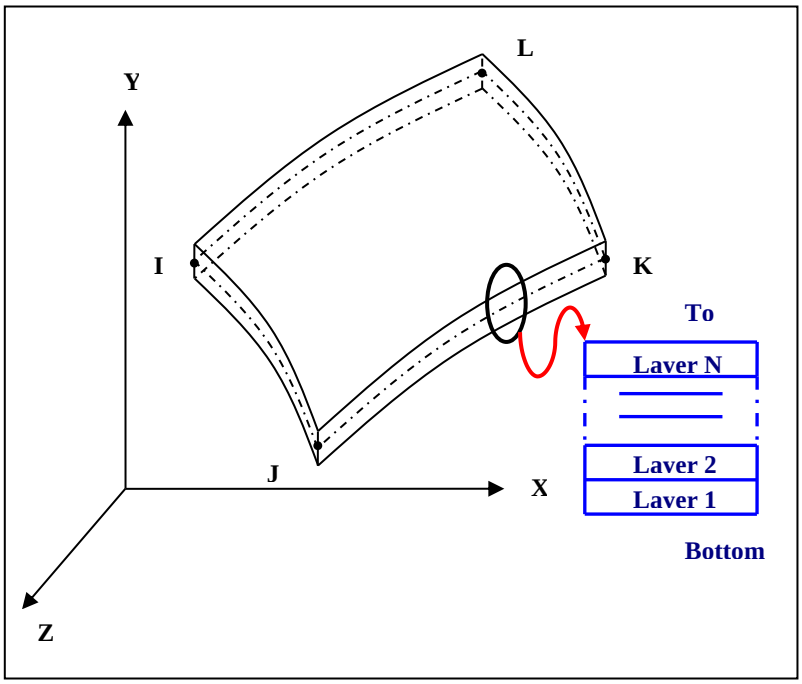

Figure 3.5 Layered quadrilateral 4-node shell element

The pipe section with the dimensions shown in Fig. 3.1 was meshed with 18144 SHELL163 elements and 19708 nodes. These types of elements are used in explicit dynamic analyses and have bending and membrane capabilities with both in-plane and normal loads permitted.

The solid steel cylinder impactor with a hemispherical tup (Fig. 3.1 and 3.4) is modeled using 6485 SOLID164 elements. The impactor is modeled as a rigid material.

b) Defining Layered Configuration

The most important characteristic of a composite material is the layers' stacking sequence. The examined GFRE composite pipe made of a fiber volume fraction of 65% and 8 plies with a ply angle of ±54.5º (Fig. 3.6) for which the reference direction coincides with the axis of the pipe [1, 2]. Through the thickness, eight integration points were used for the modeled shell elements. The 2D LS-DYNA could not capture inter-ply delamiantion [12] and in composites' delamination models, the thin solid interface is modeled as a sheet of zero thickness [7]. The calculation of the element matrices requires material properties, nodal coordinates and geometrical parameters. Any data required for the calculation of the element matrix that cannot be determined from the nodal coordinates or material properties are called "Real constants" in ANSYS [24]. In the present model, real constants are used to define the thickness of the shell elements, plies lay-up configuration and integration points. To deliver accurate results, utmost care should be considered throughout defining the shear factor (SHRF), the number of integration points through the thickness of the element (NIP), the shell thickness at each of the 4 nodes (T1-T4), the location of the reference surface (NLOC), the spacing of integration points (ESOP) and the material angle, in degrees, (BETA(i)) which must be specified for each integration point.

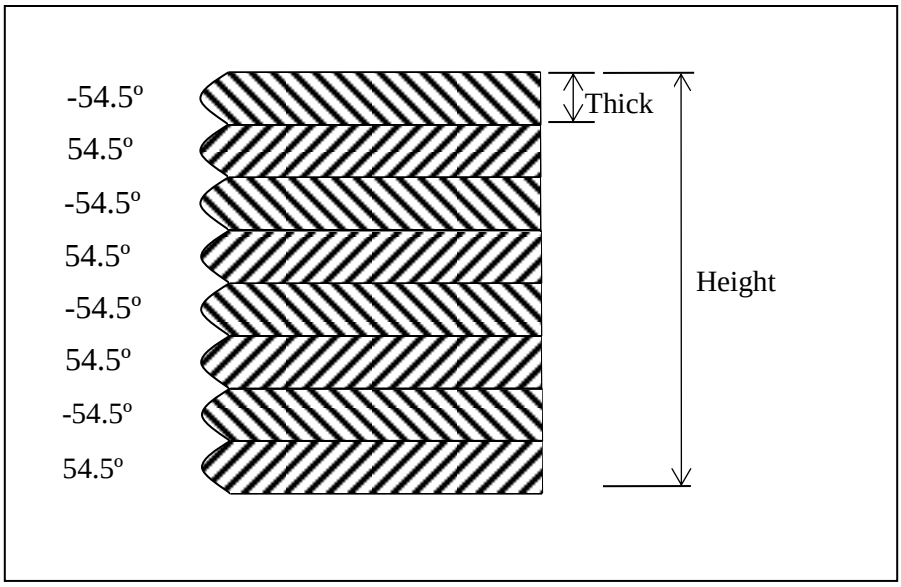

Figure 3.6 Layer configuration of GFRE pipe

3.1.3 Material Properties

The GFRE pipe is made of high strength continuous E-glass fibers and cured with amine epoxy resin. It is wound at a 54.5º helical angle and connected with the epoxy resin. Given the similarity of materials and configuration work, values in Table 3.1 and 3.2 were used [25].

Material properties used in explicit dynamic analyses differ from those used in ANSYS implicit analyses. Most explicit dynamics material models require data table input command (TB) which most often is used to define nonlinear material data. The form of the data table depends on the material model being defined [23]. In the present work, a composite material model that represents an orthotropic material was applied in the preprocessing phase. The input material properties included the elastic moduli (E_X, E_Y,

E_Z), shear moduli (GXY, GYZ, GXZ), density (DENS), and Poisson's ratios (NUXY, NUYZ, NUXZ).

Table 3.1 Material properties of E-glass/Epoxy composite [25]

E_a	40.51 GPa
E_t	13.96 GPa
G_{12}	3.10 GPa
ν_{12}	0.32
ρ	1830 kg/m^3
S_1^t	783.30 MPa
S_2^t	64 MPa
S_1^c	298 MPa
S_2^c	124 MPa
S_{12}	69 MPa
S_{23}	38 MPa

Table 3.2 Material properties of the impactor [25]

E_i	207 GPa
ν_i	0.3
ρ	8290 kg/m^3

3.1.4 Defining Boundary Conditions and Loading

Similar to the experimental test conditions [1, 2], the 300 mm long pipe section is considered to be simply supported with a span of 240 mm. The boundary conditions were used to simulate two V-block test fixtures on which the tested GFRE pipe was initially placed (Fig. 3.7). In the xy plane, the boundary conditions were such that the displacement in the z-direction and rotations in the x and y directions are restricted. Similarly, the displacement in the x-direction and rotations in y and z directions were restricted in the yz plane.

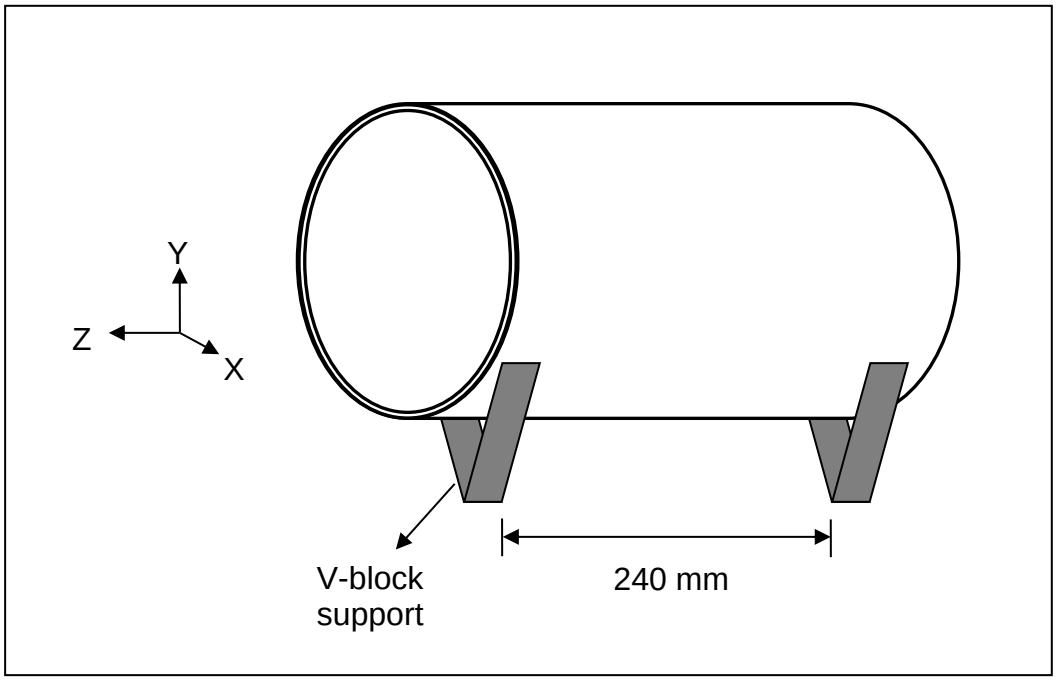

Figure 3.7 Schematic representation of GFRE pipe section on V-block supports

To simulate the experimental conditions, impact load (F) results from a freely dropped mass (m) of up to 25 kg on a node mid-span of the top surface of GFRE composite pipe were applied. In order to maintain the required impact loading, an extra weight was lumped at the end of the impactor. During the free fall stage, the impactor was simply accelerated due to gravity. To save CPU time, the analysis started just prior to hitting of the pipe by the impactor. The applied initial velocity and the vertical distance were chosen to simulate the selected impact energy assuming no friction. The velocity V_f is approximated from the law of conservation of energy where the kinetic energy before impact is set equal to the potential energy at height (H):

$$V_f = \sqrt{2GH} \qquad (3.1)$$

3.1.5 Creating Contact Surfaces

In contrast with other types of ANSYS analyses, there are no contact elements for explicit dynamic analysis. Instead, the ANSYS/LS-DYNA program can define contact between surfaces very efficiently throughout identifying the contact surfaces then the type of contact between them [23].

For this model, the contact algorithm required creating two components to represent the impactor (contact component) and the GFRE pipe (target component). Each component was linked to a material number then attached with all related elements and nodes through selecting entities. Due to the nature of this problem in which contact conditions are unpredictable, no contact algorithm was chosen. Instead, automatic surface to surface contact between the pipe and the impactor was selected and the program automatically adjusted for the changes which occur during this modeling.

Once the model was completed, its performance was tested by validating it using published FE results on Graphite /Epoxy composite with a layup which is different from that of the GFRE at hand.

3.4 Validation of FE Model

In order to validate the FE model utilized in the present study, an explicit (ANSYS/LS-DYNA) model described in section 3.3, was built specifically to simulate the numerical work performed by Yen et al. [16]. The integrated dynamic code was used to predict the load-time histories and damage for Graphite/Epoxy composite laminate pipe under impact conditions. The FE models for the pipe and the impactor were generated. The 4-node shell elements (SHELL163) and the laminated composite material model were used to model a 5 inch (127 mm) diameter pipe with 12.5 inch (317.5 mm) in length and a thickness of the 0.055 inch (1.4 mm). The solid steel cylinder impactor with 0.5 inch (12.7 mm) diameter and a hemispherical tip was modeled using 8-node brick elements (SOLID164). In order to maintain a total impact weight of 11.34 lbs (5.144 kg), an extra weight was lumped at the end of the impactor. Boundary conditions were defined to simulate two V-block test fixtures on which the test tube was initially placed. The automatic surface to surface contact between the pipe and the impactor was used for the same reason mentioned earlier.

The composite pipe consisted of a [30/-30/90/90/30/-30/90/90] lay-up configuration for which the reference direction coincides with the axis of the pipe and the last [90] ply was

the outermost layer. Eight integration points were used through the thickness for the elements in the area adjacent to the initial impact point. The material properties values in Table 3.3 and Table 3.4 were used [16].

Table 3.3 Material properties of Graphite /Epoxy composite [16]

E_a	165.5 GPa
E_t	10.3 GPa
G_{12}	5.5 GPa
ν_{12}	0.32
ν_{12}	0.36
ρ	1600 kg/m^3
S_1^t	2.55 GPa
S_2^t	0.04 GPa
S_1^c	1.5 GPa
S_2^c	0.14 GPa
S_{12}	0.12 GPa
S_{23}	0.07 GPa

Table 3.4 Material properties of the impactor [16]

E_i	207 GPa
ν_i	0.3
ρ	8290 kg/m^3

Impact force is a very important parameter in the prediction of structure damage under drop weight impact. Its variation with time is essential for prediction of damage. As a result, the computed contact force histories were compared to the numerical contact force results of Yen et al. [16]. Figures 3.8 and 3.9 show the impact load vs. time for velocities of 1.195 m/s (3.92 ft/sec) and 1.548 m/s (5.08 ft/sec), respectively.

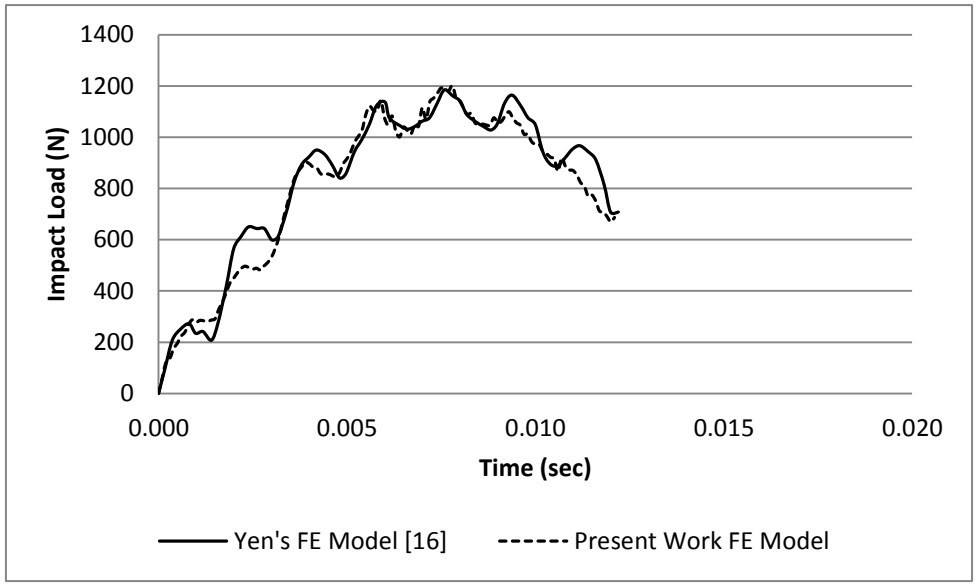

Figure 3.8 FE code validation at V_f = 1.195 m/s

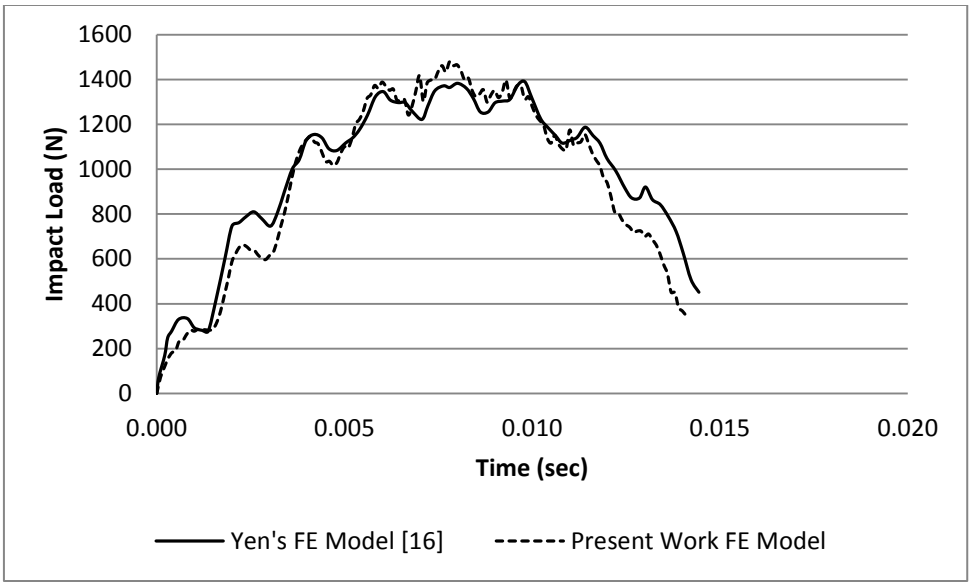

Figure 3.9 FE code validation at V_f =1.548 m/s

For both velocities, excellent agreement was found between Yen's numerical model results and the present FE model results having similar curve morphology for impact load-time plots with differences within numerical approximation. Within this time range, the analyses provide approximately the same frequencies and peak-to-peak magnitudes of the experimental data in both cases. This correlation validates the model and supports the use of the chosen contact model.

It is worth mentioning that the selection of the correct boundary conditions and refining of mesh play an important role in defining the load-time trace. Figure 3.10 shows a comparison of load-time profile for a previously developed FE model with a coarser mesh and different boundary conditions at an impact velocity of 1.195 m/s.

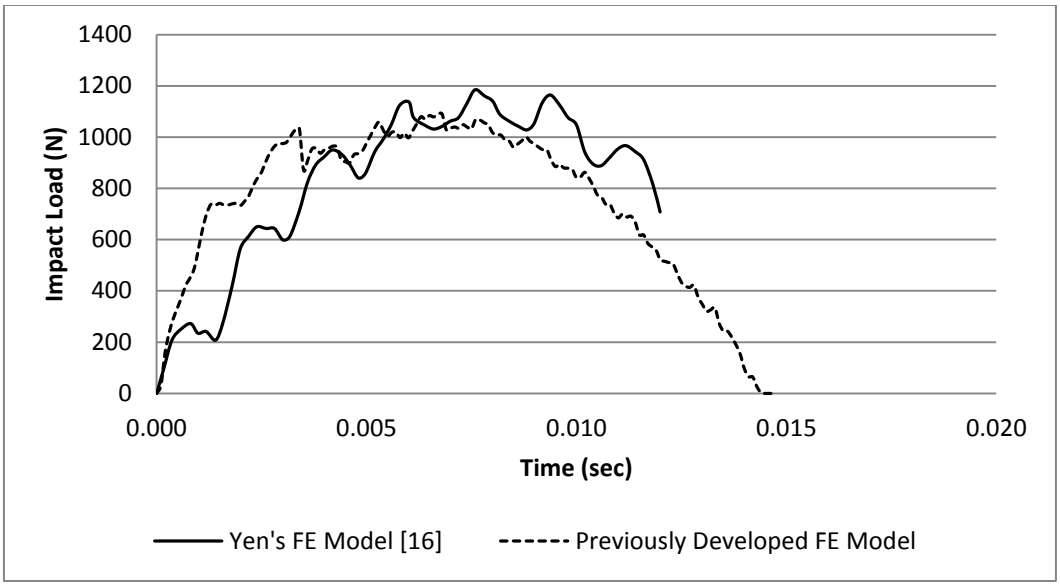

Figure 3.10 The previously developed FE code validation at V_f = 1.195 m/s

Therefore, the modified FE model will be applied to the problem at hand which consists on investigating the behavior of GFRE pipe under low and high energy impact. The analysis will include also the quantification of damage to the pipe structure as well as a pipe wall thickness effects.

CHAPTER 4

RESULTS AND DISCUSSION

4.1 Theoretical Background of Damage Analysis

As reported by several researches [1, 2, 16, 17, 26], the damage modes that may occur in a composite structure subjected to transverse impact loading include: matrix tensile cracking, matrix compressive/shear failure, fiber breakage (tensile or compressive) and ply separation (delamination). The failure criteria based on the 3D stresses in a unidirectional composite layer, with improved progressive failure modeling capability that were developed by Yen et al. [16], Kim et al. [17] and Choi and Chang [26] were applied in this study. The occurrence of delamination is subsequent to the layer matrix failure. The failure initiation criteria are applied directly to characterize the progression of the associated failure modes. Thus, all six stress components are necessary to characterize and discriminate among the various possible failure modes. The failure criteria are expressed in terms of stress components based on ply configuration (σ_1, σ_2, σ_3, τ_{12}, τ_{23}, τ_{31}) with 1, 2 and 3 denoting the fiber, in-plane transverse and out-of-plane directions, respectively.

4.1.1 Fiber Failure Modes

The fiber tensile mode is assumed to depend only on the axial stress, (σ_1), and the fiber tensile failure occurs when:

$$\left[\frac{\sigma_1}{S_1^t}\right]^2 = 1 \quad \text{for } (\sigma_1 > 0) \tag{4.1}$$

This criterion is used to predict a failure mode characterized by fiber breakage. When fiber failure in tension is predicted in a layer, the load carrying capacity of that layer is completely eliminated. The loss of stiffness is indicated by reducing E_a, E_t, G_{12}, and G_{23} all to zero.

The compressive fiber mode failure criterion is governed by the maximum stress criterion:

$$\left[\frac{\sigma_1}{S_1^c}\right]^2 = 1 \quad \text{for } (\sigma_1 < 0) \tag{4.2}$$

This criterion is used to predict a failure mode characterized by fiber buckling. For compressive fiber failure, the layer is assumed to carry a residual axial load, while the transverse load carrying capacity is reduced to zero, $E_t = G_{12} = G_{23} = 0$. When the compressive axial stress in a layer reaches the S_1^c, the axial layer stress is assumed to be reduced to S_1^{RC}.

4.1.2 Matrix Failure Modes

Matrix mode failure is characterized by cracks running parallel to the fibers. Both matrix mode failure criteria assume quadratic interactions between the transverse stresses (both

in-plane σ_2 and through the thickness σ_3), the maximum shear stress in the transverse plane, and the maximum axial shear stress.

The matrix tensile matrix failure is predicted when:

$$F_t^2 = \left[\frac{\sigma_2+\sigma_3}{S_2^t}\right]^2 + \frac{(\tau_{23}^2-\sigma_2\sigma_3)}{S_{23}^2} + \frac{(\tau_{12}^2+\tau_{31}^2)}{S_{12}^2} = 1 \quad \text{for } (\sigma_2+\sigma_3) > 0 \qquad (4.3)$$

The compressive failure criterion, which is also referred to as compressive/shear failure criterion, is a simple quadratic interaction between the maximum transverse and axial shear stresses. This failure mode is predicted by:

$$F_c^2 = \frac{\left[\frac{\sigma_2-\sigma_3}{2}\right]^2+\tau_{23}^2}{S_{23}^2} + \frac{(\tau_{12}^2+\tau_{31}^2)}{S_{12}^2} = 1 \text{ for } (\sigma_2+\sigma_3) < 0 \qquad (4.4)$$

There is no stiffness reduction assumed after matrix failure occurred because transverse matrix cracks alone usually do not have significant effect on the laminate stiffness as can be seen from the values of the moduli of elasticity illustrated in Table 3.1.

4.1.3 Delamination Modes

A delamination is a crack which runs in the resin-rich area between plies with different fiber orientation. Delamination caused by transverse impact usually occurs after an energy threshold has been reached.

The tensile/shear delamination mode is given by:

$$S^2F_t^2 = 1 \quad \text{for } (\sigma_2+\sigma_3) > 0 \qquad (4.5)$$

While the compressive/shear delamination mode is given by:

$$S^2 F_c^2 = 1 \quad \text{for } (\sigma_2 + \sigma_3) < 0 \tag{4.6}$$

Where S is used as a scale factor which can be determined from fitting the analytical prediction to experimental data for the delamination area. A value ranging from 1.8 to 2.0 has been shown to be adequate from experiments [26].

When delamination is predicted, the transverse modulus, the axial and transverse shear moduli are reduced to zero in the layer with matrix damage, i.e. $E_t = G_{12} = G_{23} = 0$ while the layer's axial modulus is unchanged.

4.2 Impact Effects on GFRE Pipes with 6 mm Wall Thickness

The present work simulates the low-velocity impact experimental tests performed using an instrumented drop weight impact test machine (DYNATUP 9250G) to evaluate the impact strength of GFRE composite pipes [1, 2]. The ANSYS/LS-DYNA integrated dynamic code that is developed and validated in section 3.2 was used to predict the load-time, deflection, energy histories and failure of GFRE composite pipes under impact energy of 12 J, 35 J, 80 J and 110 J. In the experiments, these impact energy levels were found to result in damages ranging from crack initiation to total penetration [1, 2].

4.2.1 GFRE pipe under impact energy of 12 J

Figure 4.1 (a) describes the impact load variation with time obtained for an impact energy of 12 J. The curve shows two sharp load drops during the loading part of the impact

event. These drops which occurred at times, t = 0.0004 and 0.0015 seconds are indications of initiation of matrix and fiber damages. A similar observation was made by Yen et al. [16]. Higuchi et al. [27] reported that compressive deformation initially absorbs large proportion of the impact energy prior to the start of the progressive buckling. The damage in the structure may have started with epoxy damage such as matrix cracks, since the strength properties of matrix are much less than those of the glass fibers.

The above mentioned GFRE pipe failure modes were verified by applying the damage analysis explained in section 4.1. The computed stresses were used with equations 4.1 to 4.6 to predict the type of damage occurring in the composite. A sample of the excel program developed for the purpose is depicted in Appendix I. Figure 4.1 (c) shows the predicted damage morphology for 8 layers of GFRE pipe under the impact energy of 12 J. The application of the above criteria revealed that matrix cracking started early (t = 0.0004 sec) in layers 1, 2, 7 and 8 followed by similar damage in layers 3 and 4 while no cracks were detected on layers 5 and 6. This is mainly due to the fact that the bending stress is minimal near the center of the pipe wall. Matrix failure in the upper layers (7 and 8) is caused by compression while tension failure may have occurred in lower layers (1 and 2). Similar to the observations made by Yen et al. [16] delamination was estimated to exist along with matrix cracking. The fiber breakage initiation occurred on the outer layer (8) at t = 0.0015 to 0.0022 sec. This is probably caused by high compression stresses. The described damages are believed to be the main reasons behind the observed drops in load (Fig. 4.1 (a)).

4.2.2 GFRE pipe under impact energy of 35 J

The load-time curve obtained under the impact energy of 35 J is shown in Fig. 4.1 (b) along with the load trace obtained under 12 J (Fig. 4.1 (a)). These results show that for 35 J, the first sharp drop in the load happened around 0.0005 sec very close to 0.0004 sec for 12 J. It can be seen that the higher the impact energy the higher the maximum impact load and that the load trace under 35 J displays progressive unloading sequence. Unlike the unloading event for 12 J which was mainly elastic, a number of small but sharp load drops are observed to occur, at 35 J, in the load-time response slightly after the maximum load indicating more damage is happening at the maximum load and during unloading.

Figure 4.1 (d) shows that, for 35 J, matrix cracking started early (at about t = 0.0006 sec) on layers 1, 7 and 8, followed by similar damage on layers 2, 4 and 6 while no cracking occurred on layers 3 and 5. The probable causes for these damages are explained earlier. As the impact time increased (t = 0.0018 sec), more matrix cracking happened on layers 1 and 4. Similar to the results obtained for 12 J (Fig. 4.1 (c)), delamination started at the same time with matrix cracking. The fiber breakage initiation occurred later between t = 0.0019 and 0.0023 sec on the inner layer and between t = 0.0019 and 0.0026 sec on the outer layers. The severity of fiber breakage increased gradually towards the outer layers of the laminate. It should be mentioned that the impactor may have only partially penetrated the pipe wall at 35 J.

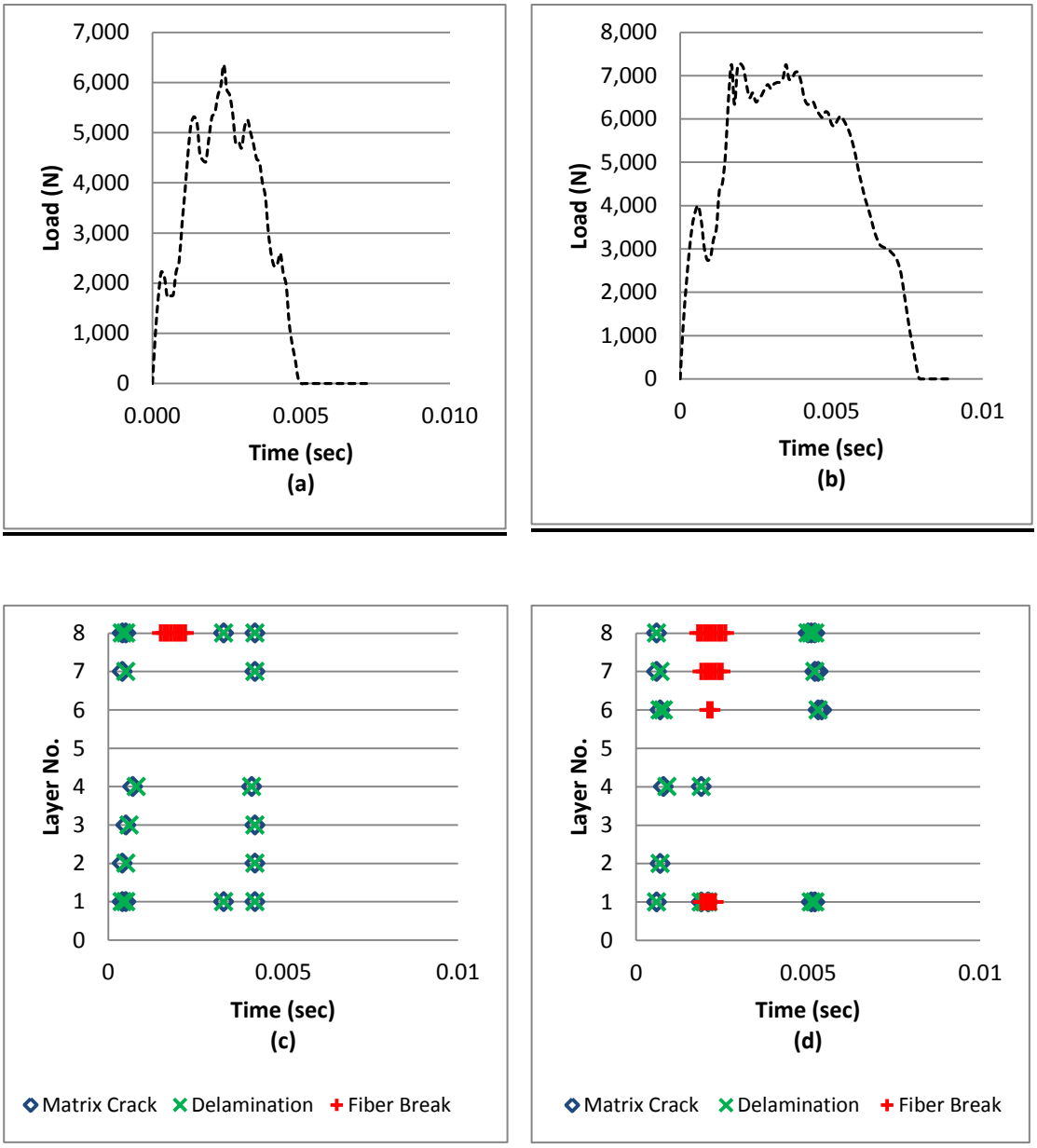

Figure 4.1 Load-time trace and layer damage under impact energy of 12 J (a and c) and 35 J (b and d)

4.2.3 Behavior of GFRE pipe wall under high impact energy (80 J and 110 J)

The load-time curve obtained under the impact energy of 80 J and 110 J are shown in Fig. 4.2 (a) and (b). These results show that the first sharp drop in the load happened around

0.0006 sec. Under continuous loading, the progression of the damage had to continue in the fibers through the thickness of the structure causing compressive fiber failure. This damage had increased with the increase of the impact load. As a result, a permanent damage caused to the structure has led to the reduction in the impact force and that the load trace displays progressive unloading sequence. Evci and Gulgec [28] reported similar findings in their experimental work.

Figure 4.2 (c) shows that, for higher impact energy of 80 J, matrix cracking started early (at about t = 0.0006 sec) on layers 1, 7 and 8, followed by similar damage on layers 2, 4, 5 and 6 while no cracking occurred on layer 3. The probable causes for these damages are explained earlier. As the impact time increased (t = 0.0015 sec), more matrix cracking happened on layer 1. Similar to the results obtained for 12 J and 35 J (Fig. 4.1 (c and d)), delamination started at the same time with matrix cracking. The fiber breakage initiation occurred later between t = 0.0016 and 0.0021 sec on the inner and the outer layers. The severity of fiber failure increased gradually towards the outer layers of the laminate. Under impact energy of 80J, the impactor may have only partially but with more sever penetration through the pipe wall compared to the impact energy of 35 J.

As the energy of impact increased to 110 J (Fig. 4.2 (d)), matrix cracking started early (at about t = 0.0006 sec) on layers 1 and 8, followed by similar damage on layers 2, 3, 4, 5, 6 and 7. As the impact time increased (t = 0.001 sec), more matrix cracking happened on layer 1. Similar to the results obtained from previous impact energies of 12 J, 35 J and 80 J, delamination started at the same time with matrix cracking. The fiber breakage initiation occurred later between t = 0.0018 and 0.0023 sec on the inner and the outer

layers. The severity of fiber failure increased gradually towards the inner and the outer layers of the laminate. Under impact energy of 110 J, the impactor caused full penetration through the pipe wall.

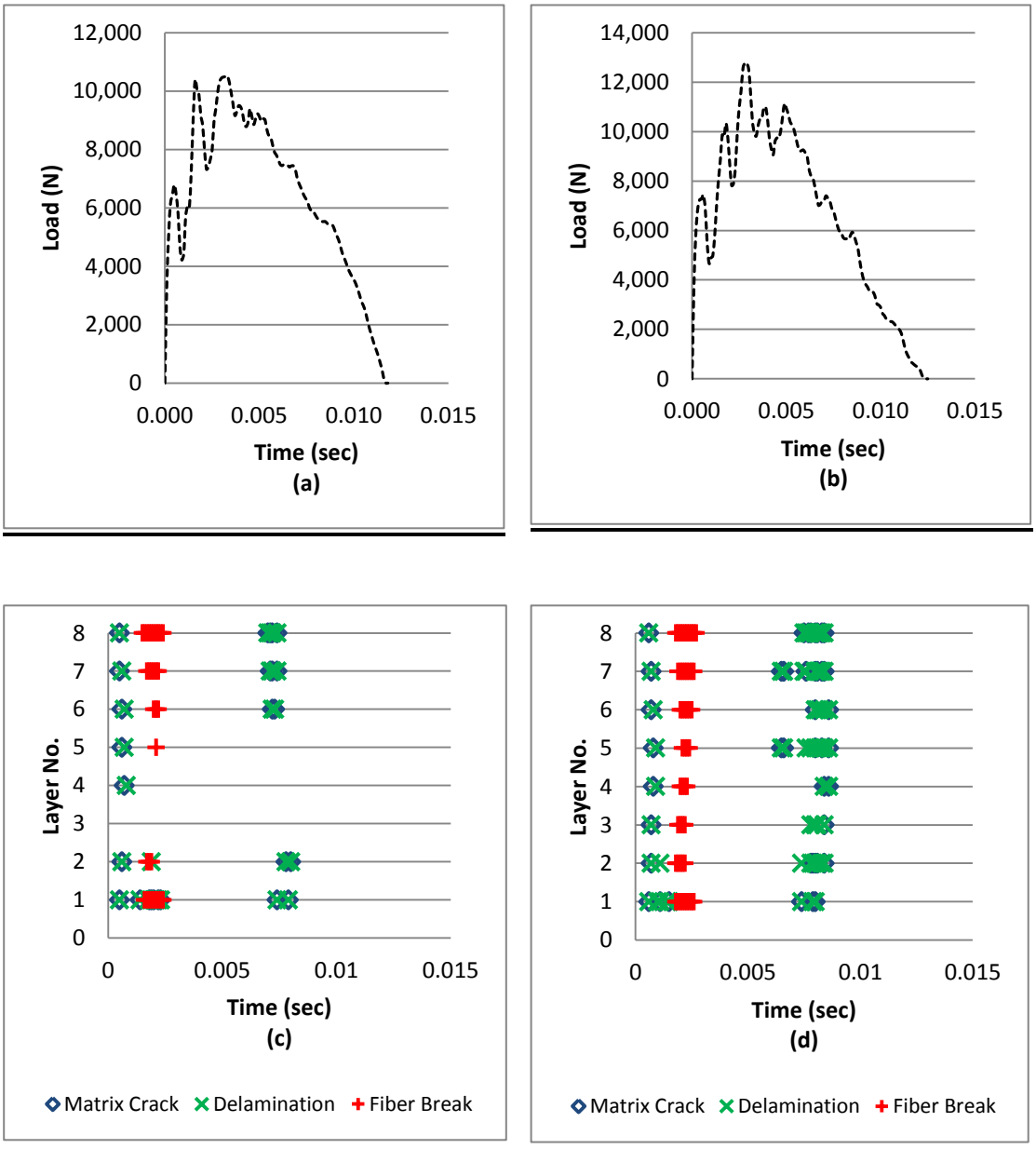

Figure 4.2 Load-time trace and layer damage under impact energy of 80 J (a and c) 80 J and 110 J (b and d)

Figures 4.3 and 4.4 show examples of the stress distribution resulting from the impact energy of 12 J and 80 J on the top surface of the GFRE pipe impacted area. The red coded color shown in these two figures represents the area where the fiber breakage occurred because the hoop stress value exceeded the compressive strength value of the fibers.

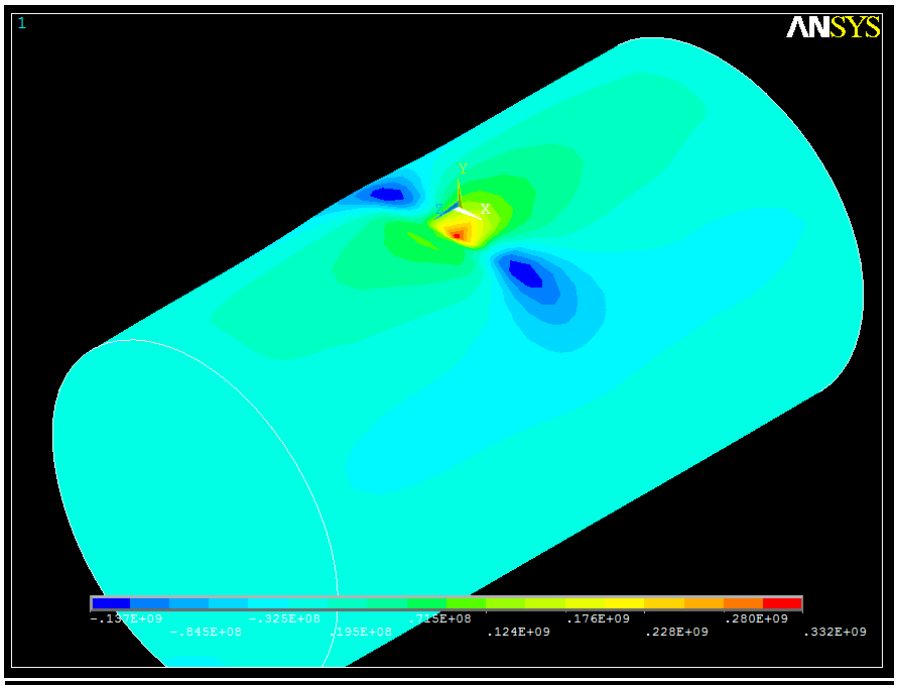

Figure 4.3 Hoop stress distribution on the impacted area of GFRE pipe under impact energy of 12 J

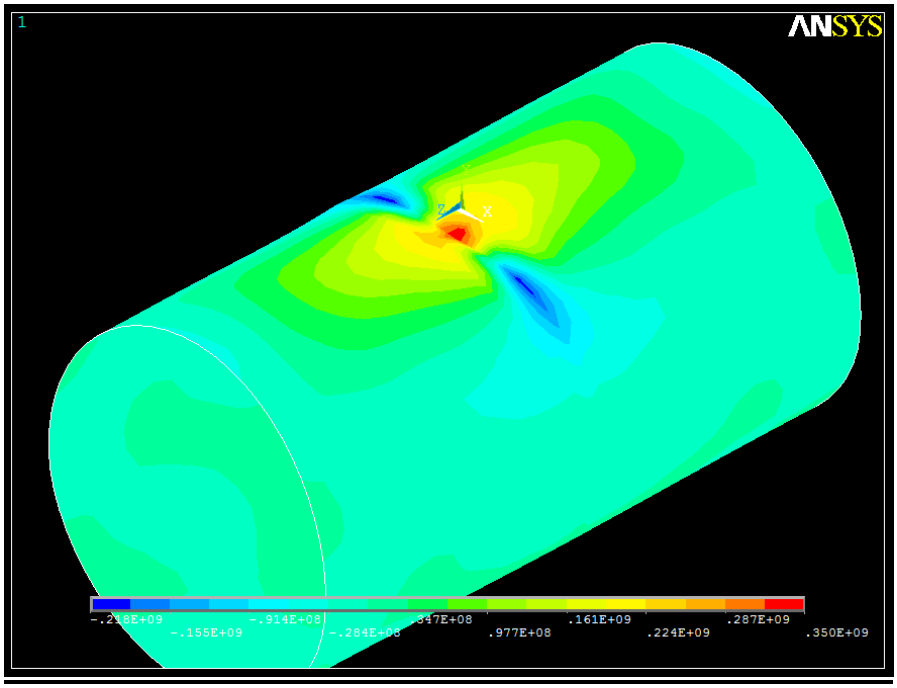

Figure 4.4 Hoop stress distribution on the impacted area of GFRE pipe under impact energy of 80 J

Collectively, Fig. 4.5 (a) shows the impact energy of 12 J, 35 J, 80 J and 110 J along with the caused deflection of the GFRE pipe at the top surface of the impacted area (Fig. 4.5 (b)). The maximum deflection under the impact energy of 12 J was 3.42 mm and the maximum deflection under the impact energy of 35 J was 6.67 mm; in both cases the pipe recovered to the conditions before the impact. In contrast, the GFRE pipe tested under the impact energy of 80 J and 110 J had permanent damages that did not allow for the pipe to recover to its original shape. The recorded maximum deflections were 19 mm and 35.1 mm, respectively.

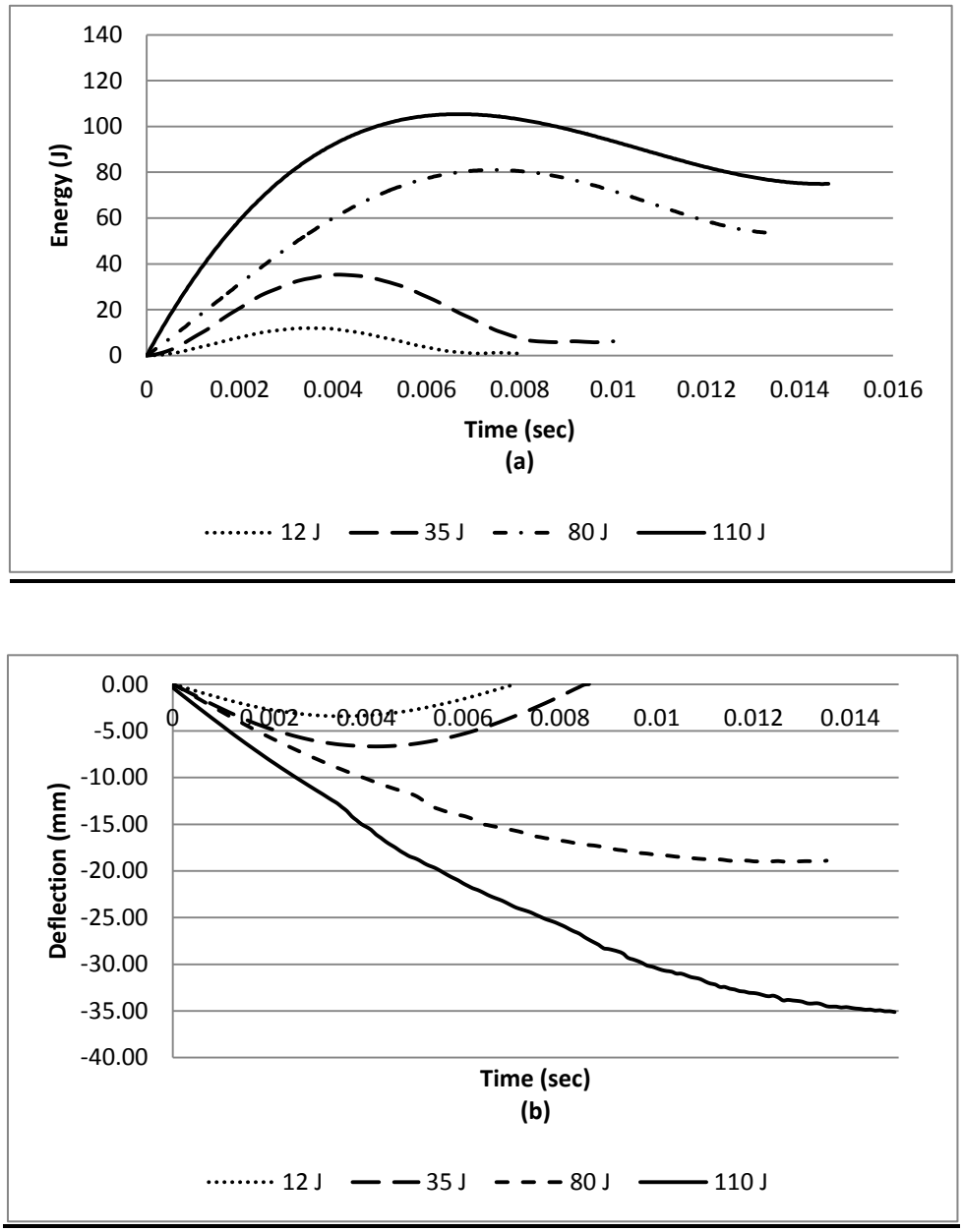

Figure 4.5 (a) Impact energy of 12 J, 35 J, 80 J and 110 J along with the caused (b) deflection-time of the GFRE pipe

4.3 Comparison of FE Results with Experimental Data

Figure 4.6 (a and b) shows good agreement between the experimental obtained by Naik [1] and Khan et al. [2] and the present FEA results. The output curves profile for impact load vs. time is similar to that obtained experimentally. Within this time range, the FE analyses provide approximately the same frequencies and peak-to-peak magnitudes as the experimental data, especially for the low impact energies of 12 and 35 J. This correlation further validates the model and supports the use of the chosen contact model. The results of this work may serve as the basis for the future research to optimize the GFRE pipes manufacturing processes.

For high impact energies, the difference between the experimental and FEA results for peak impact force varied from 10% at 80 J to 18% at 110 J. It is known that the accuracy of the FEA reduces with increase in impact velocity. This implies that since kinetic energy varies as a square of the velocity, the effect of the difference in the final velocities (between experimental and FEA), could be large and indicate that the FEA energy dissipated in the fracture of the laminate is less than the value obtained in the experimental work. A similar finding was reported by Okoli and Abdul-Latif [4].

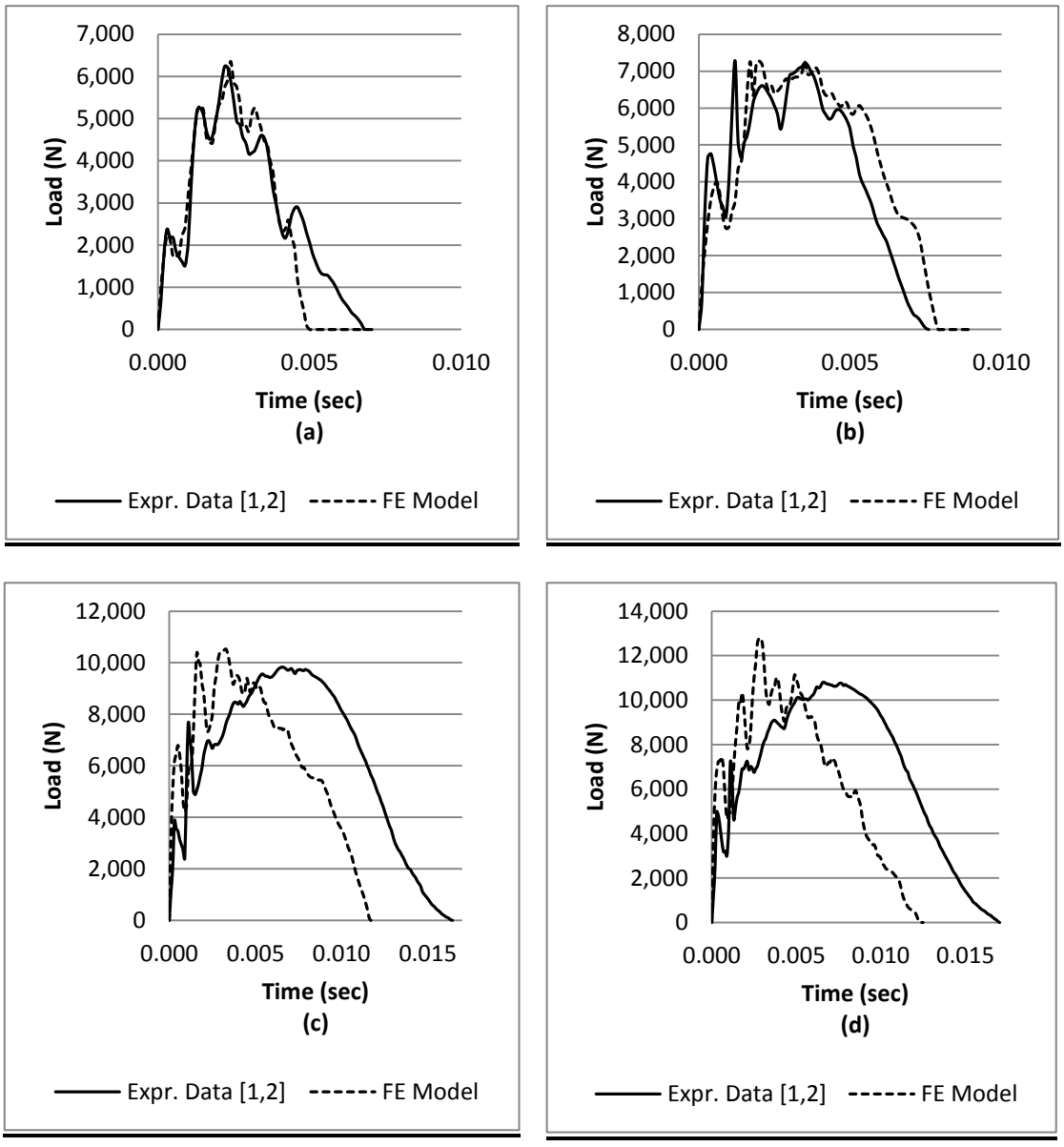

Figure 4.6 Experimental results validation under impact energy of (a) 12 J (b) 35 J (c) 80 J and (d) 110 J

4.4 Impact Effects on GFRE Pipes with 4.5 mm Wall Thickness

The present work also targets a filament wound GFRE pipe with different thickness. Similar low-velocity impact simulation were carried out using ANSYS/LS-DYNA

integrated dynamic code to predict the load, deflection and energy histories for GFRE pipes with a thickness of 4.5 mm under impact energy of 12 J, 35 J, 80 J and 110 J. These impact energy levels were found to result in damages ranging from crack initiation to total penetration at impact energy of 80 J and 110 J. The FE models for the pipes and the impactor were generated as described in Chapter 3.

4.4.1 Behavior of GFRE pipe wall under high impact energy (12 J and 35 J)

The load-time curve obtained under the impact energies of 12 J and 35 J is shown in Fig. 4.7 (a) and (b). These results show that for 12 J and 35 J, the first sharp drop in the load happened around 0.0004 and 0.0006 sec, respectively. It can be seen that the higher the impact energy the higher the maximum impact load and that the load trace under both 12 J and 35 J displays progressive unloading sequence. Similar to what was observed for 6-mm thick pipe, the unloading event for 12 J which was mainly elastic while a number of small but sharp load drops are observed to occur, at 35 J, slightly after the maximum load indicating more damage is happening at the maximum load and during unloading.

Figure 4.7 (a and c) shows that, for 12 J, matrix cracking started early (at about t = 0.0004 sec) on layers 1 and 8, followed by similar damage on layers 2, 3, 4 and 7 while no cracking occurred on layers 5 and 6. The probable causes for these damages are as explained earlier for the 6-mm thick pipe wall. Similar to the results obtained for 12 J (Fig. 4.1 (c)), delamination started at the same time with matrix cracking. The fiber breakage initiation occurred later between t = 0.0017 and 0.0038 sec on the outer layers. The severity of fiber failure increased gradually towards the outer layers of the laminate.

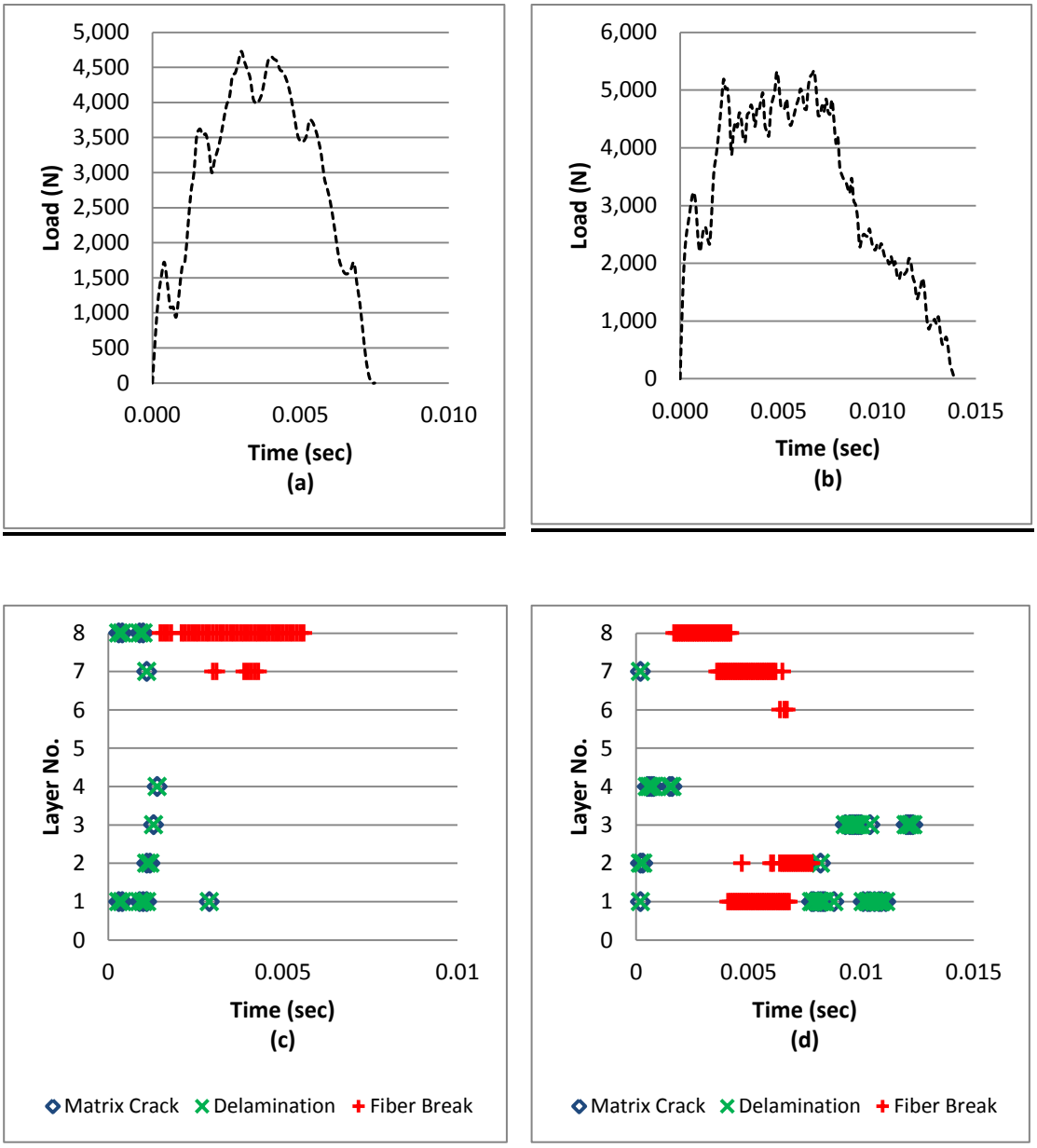

Figure 4.7 Load-time trace and layer damage under impact energy of 12 J (a and c) and 35 J (b and d)

Figure 4.7 (b and d) shows that, for 35 J, matrix cracking started early (at about t = 0.0006 sec) on layers 1, 2, 7 and 8, followed by similar damage on layers 3, 4 and 6 while no cracking occurred on layer 5. Similar to the results obtained for the 6-mm thick

pipe wall at the impact energy of 35 J (Fig. 4.1 (d)), delamination started at the same time with matrix cracking. The fiber breakage initiation occurred later between t = 0.0039 and 0.0062 sec on the inner layer and between t = 0.0018 and 0.0042 sec on the outer layer. The severity of fiber failure increased gradually towards the outer layers of the laminate. It should be mentioned that the impactor may have only partially penetrated the pipe wall at 35 J.

4.4.2 Behavior of GFRE pipe wall under high impact energy (80 J and 110 J)

The load-time curve obtained under the impact energies of 80 J and 110 J are shown in Fig. 4.8 (a) and (b). These results show that the first sharp drop in the load happened around 0.0007 sec. As proved earlier, the major mode of failure for this impact loading scenario was compressive fiber failure due to the damage to the fibers through the thickness of the laminate which in turn caused the reduction in the load carrying capacity of the pipe.

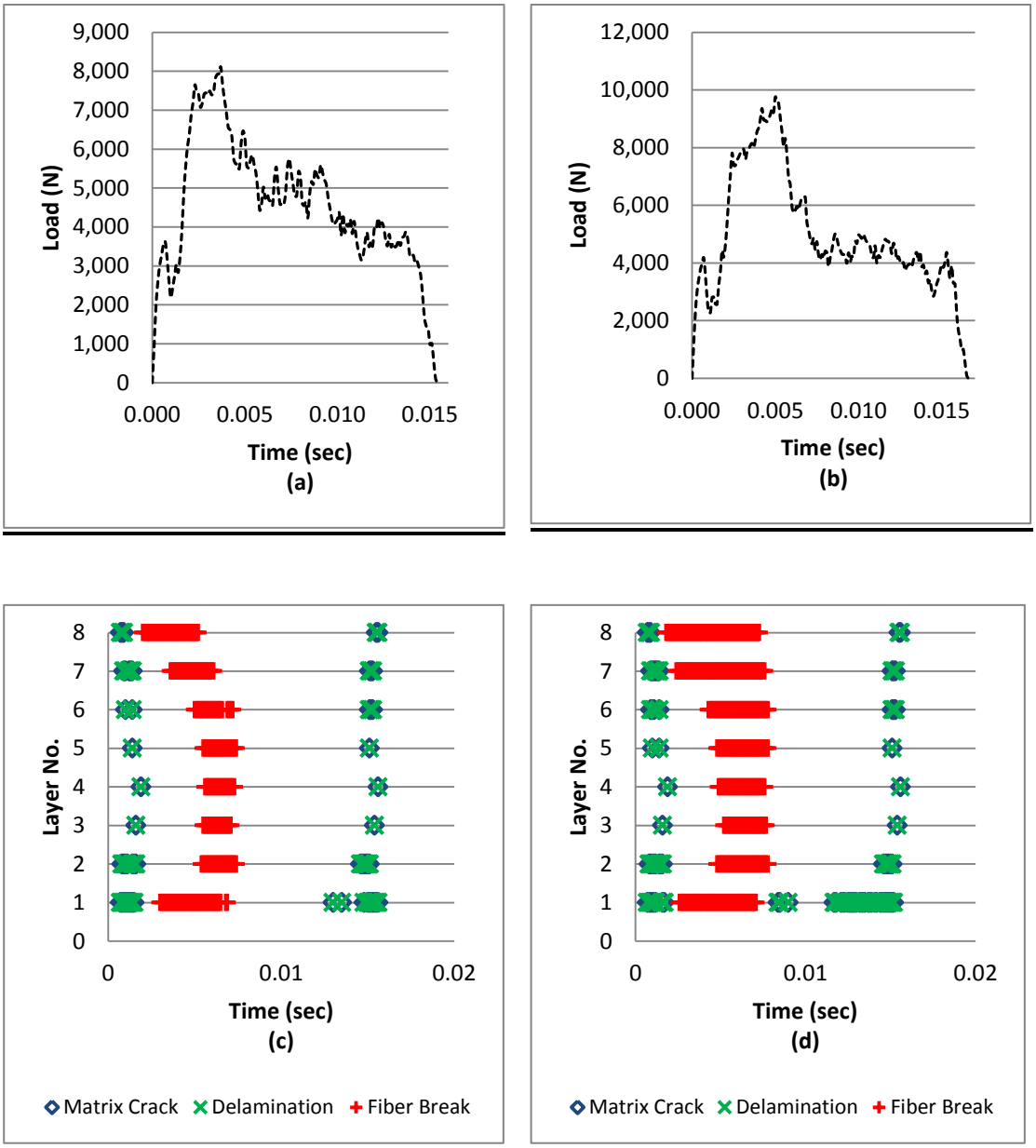

Figure 4.8 Load-time trace and layer damage under impact energy of 80 J (a and c) and 110 J (b and d)

Figure 4.8 (c) shows that, for higher impact energy of 80 J, matrix cracking started early (at about t = 0.0007 sec) on layers 1, 2, 7 and 8, followed by similar damage on layers 3, 4, 5 and 6. As reported earlier, delamination started at the same time with matrix

cracking. The fiber breakage initiation occurred later between t = 0.003 and 0.0068 sec on the inner layer and between t = 0.002 and 0.0052 sec on the outer layer. The severity of fiber failure increased gradually towards the outer layers of the laminate. Under impact energy of 80 J, the impactor caused full penetration through the pipe wall.

As the energy of impact increased to 110 J (Fig. 4.8 (d)), matrix cracking started early (at about t = 0.0007 sec) on layers 1, 2, 7 and 8, followed by similar damage on layers 3, 4, 5 and 6. As reported earlier, delamination started at the same time with matrix cracking. The fiber breakage initiation occurred later between t = 0.0026 and 0.0071 sec on the inner layer and between t = 0.0018 and 0.0073 sec on the outer layer. The severity of fiber failure increased gradually towards the inner and the outer layers of the laminate. Under impact energy of 110 J, the impactor caused full penetration through the pipe wall.

Collectively, Fig. 4.9 (a) shows the impact energy of 12 J, 35 J, 80 J and 110 J along with the caused deflection of the GFRE pipe at the top surface of the impacted area (Fig. 4.9 (b)). The maximum deflection under the impact energy of 12 J was 5.14 mm and the maximum deflection under the impact energy of 35 J was 10.76 mm; in both cases the pipe recovered to the conditions before the impact. In contrast, the GFRE pipe tested under the impact energy of 80 J and 110 J had permanent damages that did not allow for the pipe to recover to its original shape. The maximum deflection was recorded as 20.38 mm.

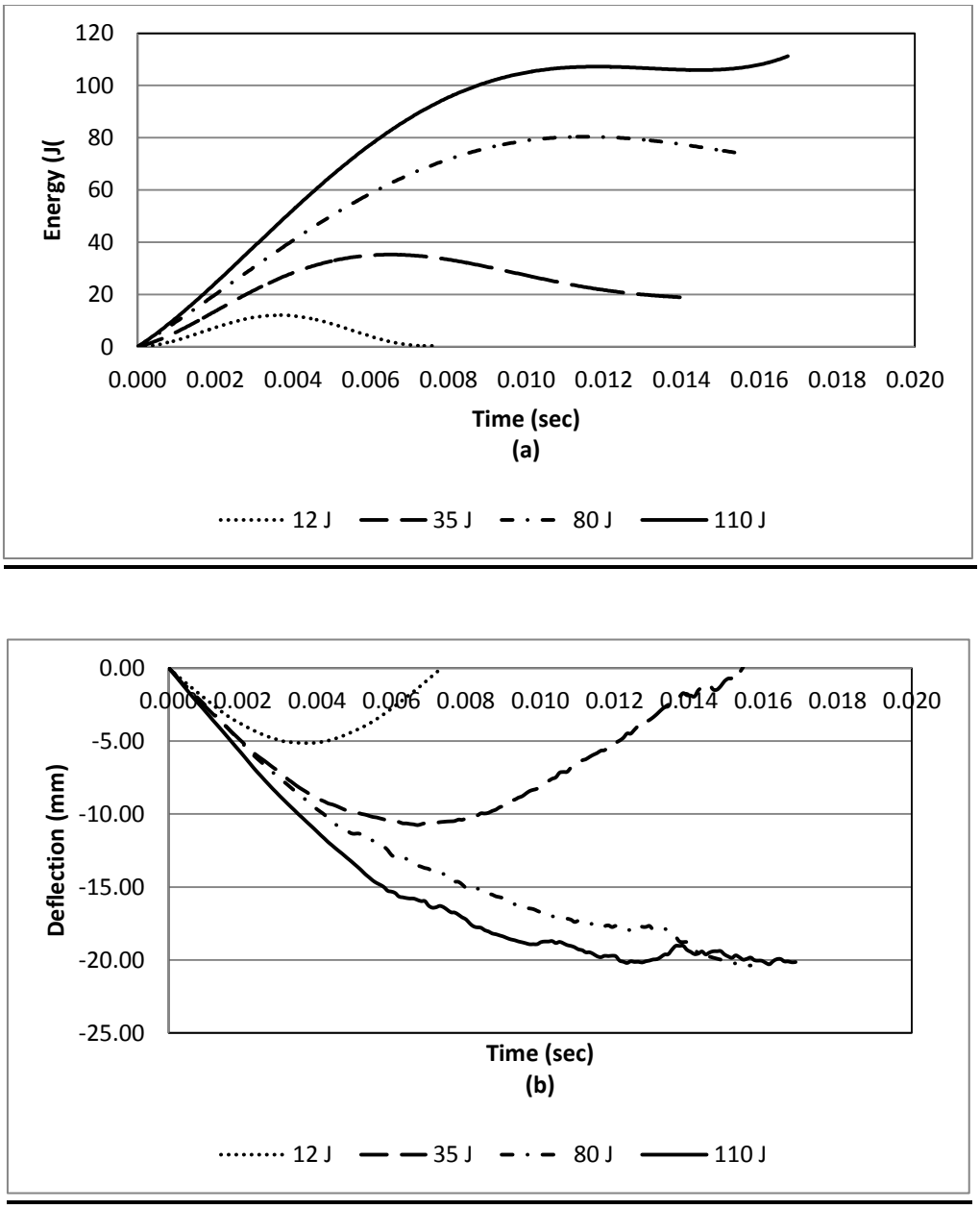

Figure 4.9 (a) Impact energy of 12 J, 35 J, 80 J and 110 J along with the caused (b) deflection-time of the GFRE pipe

4.5 Effect of Wall Thickness on the Impact Resistance of the GFRE Pipes

The filament wound GFRE pipe with two different wall thicknesses are considered in the present study to determine the effect of wall thickness on the impact resistance of the GFRE pipes. From analyzing the results for both 6 mm and 4.5 mm wall thickness GFRE pipes in sections 4.2 and 4.3, respectively, it was found that the damage started with an elastic deformation with an increase of impact loading until the occurrence of matrix cracking and delaminations. The fiber breakage happened at the maximum impact load. Some matrix cracking and delaminations occurred, mainly at intermediate and high impact energies, when the load drops off during the unloading events. Similar findings were reported by Ruhala and Engel [10]. Similar to what Hosseinzadeh et al. [19] observed for smaller wall thickness, the size of damage increases at higher impact energy. As can be inferred from the comparisons of the results of figures 4.1 and 4.2 to those of figures 4.7 and 4.8, under similar conditions and range of impact energy, the damage through 4.5 mm wall thickness GFRE pipes is more severe than for 6 mm wall thickness pipes. Figure 10 shows that the impactor caused full penetration through the 4.5 mm pipe wall under the impact energy of 80J while the fibers in layers 3 and 4 of the 6 mm pipe remained intact.

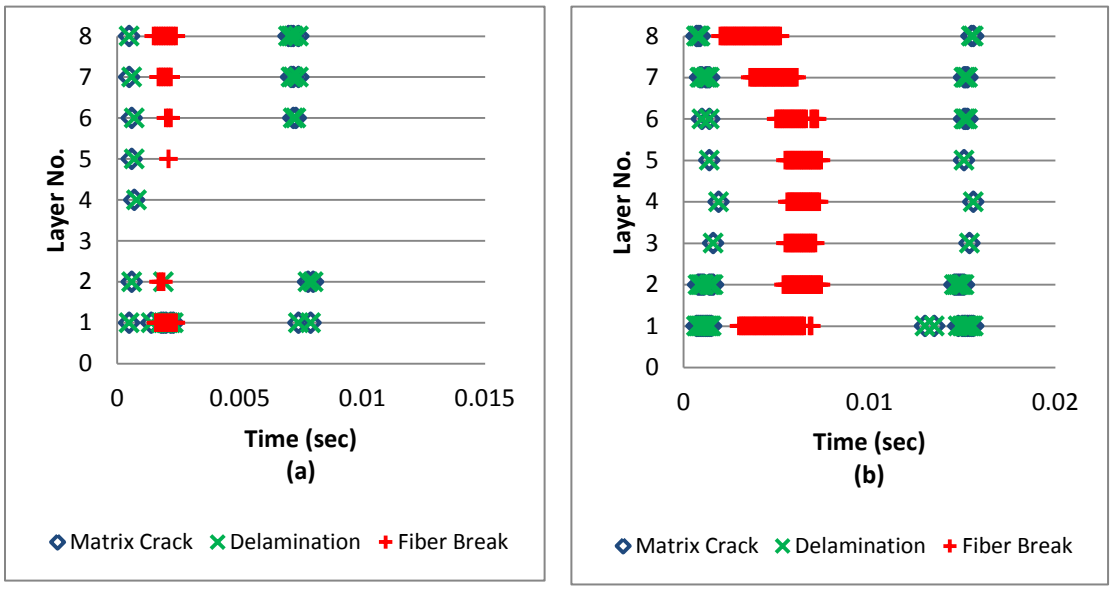

Figure 4.10 Comparison between damages caused by 80 J impact energy in (a) 6 mm and (b) 4.5 mm wall thickness GFRE pipes

CHAPTER 5

CONCLUSION AND RECOMMENDATION

5.1 Conclusion

A FE model of a 150-mm inner diameter epoxy based filament-wound E-glass fiber reinforced thermoset pipe and steel impactor was successfully developed to analyze the composite's structural behavior under low velocity impact. Load, deflection, stresses and energy histories were obtained for different impact energies (12, 35, 80 and 110 J) and for different pipe wall thicknesses (4.5 and 6.0 mm). The results obtained from the ANSYS/LS-DYNA code built for the present study were validated using published numerical and experimental results.

In the load-time traces it was observed that a reduction of the impact force happened early during the loading event, indicating the initiation of the matrix damage mode. Due to continuous loading beyond that point, there is a continuous progression of the damage to the fibers through the thickness of the structure which increases with impact load, until the time where there is a permanent damage caused to the structure and thus reduction in the impact force.

The unloading event for low impact energy was mainly elastic while at intermediate and high impact energy, a number of sharp load drops are observed to occur at or slightly

after the maximum load indicating more damage is happening at the maximum load and during unloading. This damage was quantified using the computed stresses and found to be progressive with time and space (through thickness). The deflection-time curves indicated that under 12 and 35 J the pipe wall was capable of regaining its initial shape while at higher impact energies the deformations were permanent.

The effect of pipe wall thickness study showed that under similar conditions and range of impact energy, the damage through 4.5 mm wall thickness pipe occurred earlier and was more severe than for 6 mm wall thickness pipes. The impactor caused full penetration through the 4.5 mm pipe wall under the impact energy of 80J while the penetration was only partial in the 6 mm thick pipe.

In summary, it can be concluded the FEM can be used effectively to simulate the low velocity impact scenario on composite pipe structures with closely predicting the subsequent failure.

5.2 Recommendations

Following are recommendations for any future work that would be carried out on GFRE filament-wound pipe under low velocity impact:

- The size of the crack in the laminate structure need to be measured to have a better quantification of the damage.

- The difference between the FEM and experimental results for peak impact force varied from 10% incremental at 80 J to 18% at 110 J. Further investigation could verify and possibly narrow this range. ANSYS/LS-DYNA has an element failure option. Ultimate strengths of the materials can be set so that once that stress is encountered, the element is eliminated and the load is transferred to the other elements. This requires more investigation into the failure loads of the laminates and further work with the composite layer option in ANSYS/LS-DYNA.
- There are many areas of interest in Pipelines at Saudi Aramco to be investigated which is related to the mechanical strength properties of GFRE pipes that have been installed in the service for long periods.

APPENDIX-I

Sample of Failure Analysis Raw Data (MS Excel)

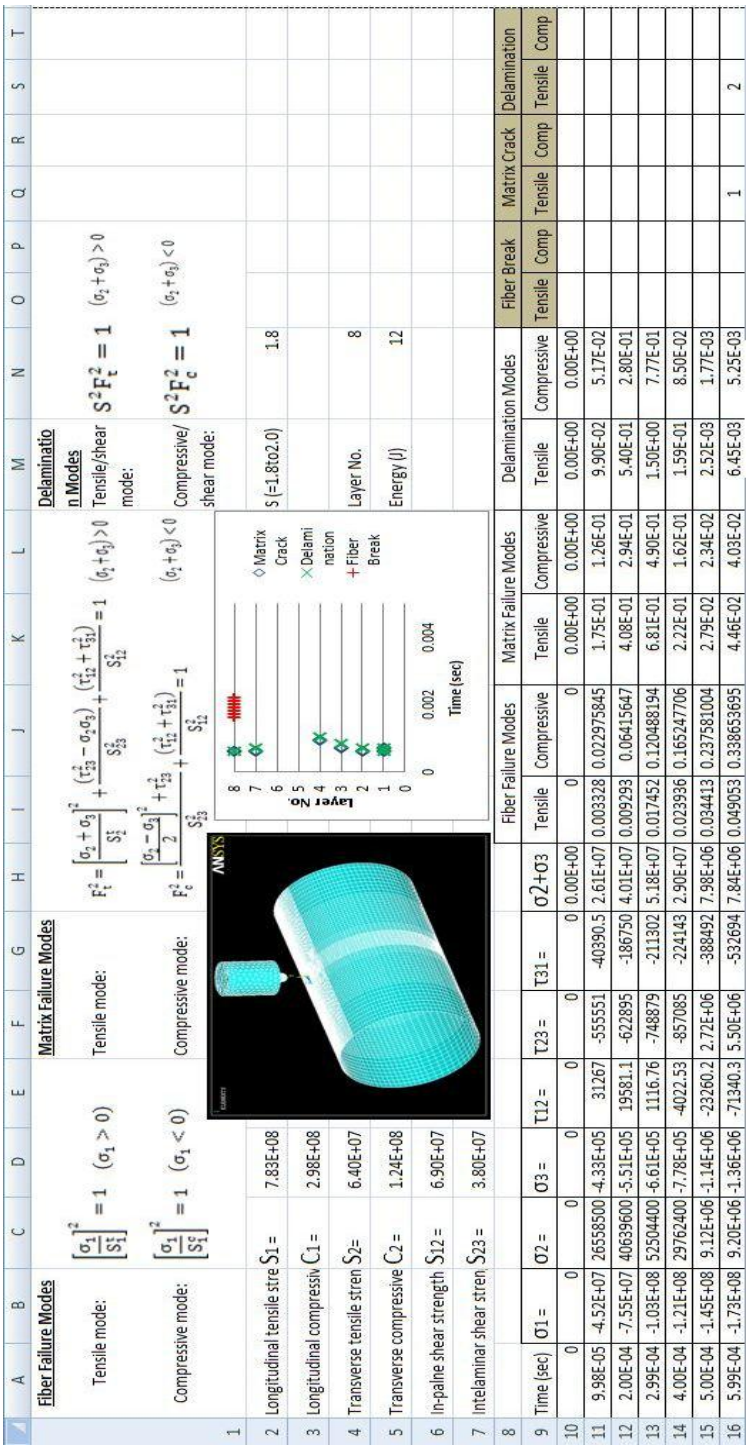

Fiber Failure Modes							Matrix Failure Modes								Delamination Modes		Fiber Break		Matrix Crack		Delamination	
Tensile mode: $\left[\frac{\sigma_1}{S_1^t}\right]^2 = 1 \quad (\sigma_1 > 0)$							Tensile mode:				$F_t^2 = \left[\frac{(\sigma_2+\sigma_3)}{S_2^t}\right]^2 + \frac{(\tau_{23}^2-\sigma_2\sigma_3)}{S_{23}^2} + \frac{(\tau_{12}^2+\tau_{31}^2)}{S_{12}^2} = 1 \quad (\sigma_2+\sigma_3)>0$			Delaminatio n Modes	Tensile/shear mode:	$S^2F_t^2 = 1 \quad (\sigma_2+\sigma_3)>0$					
Compressive mode: $\left[\frac{\sigma_1}{S_1^c}\right]^2 = 1 \quad (\sigma_1 < 0)$							Compressive mode:				$F_c^2 = \frac{\left[\frac{\sigma_2-\sigma_3}{2}\right]^2 + \tau_{23}^2}{S_{23}^2} + \frac{(\tau_{12}^2+\tau_{31}^2)}{S_{12}^2} = 1 \quad (\sigma_2+\sigma_3)<0$				Compressive/ shear mode:	$S^2F_c^2 = 1 \quad (\sigma_2+\sigma_3)<0$					
Longitudinal tensile stre	S_1 =	7.83E+08													S (=1.8to2.0)	1.8						
Longitudinal compressiv	C_1 =	2.98E+08																				
Transverse tensile stren	S_2=	6.40E+07													Layer No.	8						
Transverse compressive	C_2 =	1.24E+08													Energy (J)	12						
In-palne shear strength	S_{12} =	6.90E+07																				
Intelaminar shear stren	S_{23} =	3.80E+07																				
									Fiber Failure Modes		Matrix Failure Modes				Delamination Modes		Fiber Break		Matrix Crack		Delamination	
Time (sec)	σ_1 =	σ_2 =	σ_3 =	τ_{12} =	τ_{23} =	τ_{31} =	$\sigma_2+\sigma_3$		Tensile	Compressive	Tensile	Compressive			Tensile	Compressive	Tensile	Comp	Tensile	Comp	Tensile	Comp
0	0	0	0	0	0	0	0.00E+00		0	0	0.00E+00	0.00E+00			0.00E+00	0.00E+00						
9.98E-05	-4.52E+07	26558500	-4.33E+05	31267	-555551	-40390.5	2.61E+07		0.003328	0.022975845	1.75E-01	1.26E-01			9.90E-02	5.17E-02						
2.00E-04	-7.55E+07	40639600	-5.51E+05	19581.1	-622895	-186750	4.01E+07		0.009293	0.06415647	4.08E-01	2.94E-01			5.40E-01	2.80E-01						
2.99E-04	-1.03E+08	52504400	-6.61E+05	1116.76	-748879	-211302	5.18E+07		0.017452	0.120488194	6.81E-01	4.90E-01			1.50E+00	7.77E-01						
4.00E-04	-1.21E+08	29762400	-7.78E+05	-4022.53	-857085	-224143	2.90E+07		0.023936	0.165247706	2.22E-01	1.62E-01			1.59E-01	8.50E-02						
5.00E-04	-1.45E+08	9.12E+06	-1.14E+06	-23260.2	2.72E+06	-388492	7.98E+06		0.034413	0.237581004	2.79E-02	2.34E-02			2.52E-03	1.77E-03			1		2	
5.99E-04	-1.73E+08	9.20E+06	-1.36E+06	-71340.3	5.50E+06	-532694	7.84E+06		0.049053	0.338653695	4.46E-02	4.03E-02			6.45E-03	5.25E-03						

APPENDIX-II

Sample of FE Code (ANSYS/LS-DYNA Program)

```
!!!!!!!****************************************!!!!!
!*
/NOPR
/PMETH,OFF,0
KEYW,PR_SET,1
KEYW,PR_STRUC,1
KEYW,PR_FLUID,0
KEYW,PR_MULTI,0
KEYW,LSDYNA,1
KEYW,PR_DYNA,1
/GO
!*
/COM,
/COM,Preferences for GUI filtering have been set to display:
/COM,  Structural with LS-DYNA Explicit
!*
/PREP7
!*********************(select elements)
!*
ET,1,SHELL163
!*
KEYOPT,1,1,6
KEYOPT,1,2,1
KEYOPT,1,3,1
KEYOPT,1,4,0,
!*
ET,2,SOLID164
!************************(set real constants)
R,1
RMODIF,1,1,1,8,0.006,0.006,0.006,0.006 !LAYER COFIGURATIN (8 LAYER 54.5,
RMODIF,1,7, 0,1,54.5,0,0.125,1   !-54.5, 54.5,-54.5, 54.5,-54.5,54.5,-54.5)
RMODIF,1,13,-54.5,0,0.125,1,54.5,0
RMODIF,1,19,0.125,1,-54.5,0,0.125,1
RMODIF,1,25,54.5,0,0.125,1,-54.5,0
RMODIF,1,31,0.125,1,54.5,0,0.125,1
RMODIF,1,37,-54.5,0,0.125,1
```

```
!***********************(define material properties)
!*
MP,DENS,1,1830
MP,EX,1,40.51e9
MP,EY,1,13.96e9
MP,EZ,1,13.96e9
MP,GXY,1,3.10e9
MP,GYZ,1,1.52e9
MP,GXZ,1,3.10e9
MP,NUXY,1,0.22
MP,NUYZ,1,.14
MP,NUXZ,1,0.22
TB,COMP,1,,,,
TBDAT,1,7.78e9
TBDAT,2,0.069e9
TBDAT,3,0.783e9
TBDAT,4,0.064e9
TBDAT,5,0.124e9
TBDAT,6,8.03e-5
!*
EDMP,RIGI,2,6,7
MP,DENS,2,8290
MP,EX,2,207e9
MP,NUXY,2,0.3
EDSHELL,20,-1,0,1,1,1
!***********************(Create, mesh & refine meshing the Cylinder)
K, ,0,0,-.15,
K, ,0,0,-.14,
K, ,0,0,-.12,
K, ,0,0,-0.09,
K, ,0,0,-0.03,
K, ,0,0,-0.01,
K, ,0,0,0,
K, ,0,0,0.01,
K, ,0,0,0.03,
K, ,0,0,0.09,
K, ,0,0,0.12,
K, ,0,0,0.14,
K, ,0,0,0.15,
K, ,0,-.081,0.15,
K, ,0,-.06075,0.15,
K, ,0,-.162,0.15,
K, ,0,-.162,0.14,
K, ,0,-.162,0.12,
K, ,0,-0.162,0.09,
K, ,0,-0.162,0.03,
```

```
K, ,0,-0.162,0,
K, ,0,-0.162,-0.03,
K, ,0,-0.162,-0.09,
K, ,0,-0.162,-0.12,
K, ,0,-0.162,-0.14,
K, ,0,-0.162,-0.15,
K, ,0,-.06075,-0.15,
K, ,0,-.081,-0.15,
/VIEW,1,1
/ANG,1
/REP,FAST
LSTR,       1,       2
LSTR,       2,       3
LSTR,       3,       4
LSTR,       4,       5
LSTR,       5,       6
LSTR,       6,       7
LSTR,       7,       8
LSTR,       8,       9
LSTR,       9,       10
LSTR,       10,       11
LSTR,       11,       12
LSTR,       12,       13
FLST,2,12,4,ORDE,2
FITEM,2,1
FITEM,2,-12
FLST,8,2,3
FITEM,8,14
FITEM,8,28
AROTAT,P51X, , , , , ,P51X, ,360,9,
!*
!*
TYPE,   1
MAT,       1
REAL,       1
ESYS,       0
SECNUM,
!*
FLST,2,4,5,ORDE,4
FITEM,2,6
FITEM,2,-7
FITEM,2,102
FITEM,2,-103
AESIZE,P51X,0.015,
!*
FLST,2,4,5,ORDE,4
```

```
FITEM,2,5
FITEM,2,8
FITEM,2,101
FITEM,2,104
AESIZE,P51X,0.015,
!*
FLST,2,16,5,ORDE,8
FITEM,2,4
FITEM,2,9
FITEM,2,16
FITEM,2,-21
FITEM,2,88
FITEM,2,-93
FITEM,2,100
FITEM,2,105
AESIZE,P51X,0.015,
!*
FLST,2,22,5,ORDE,10
FITEM,2,3
FITEM,2,10
FITEM,2,15
FITEM,2,22
FITEM,2,27
FITEM,2,-34
FITEM,2,87
FITEM,2,-94
FITEM,2,99
FITEM,2,106
AESIZE,P51X,0.02,
!*
FLST,2,32,5,ORDE,16
FITEM,2,2
FITEM,2,11
FITEM,2,14
FITEM,2,23
FITEM,2,26
FITEM,2,35
FITEM,2,38
FITEM,2,-47
FITEM,2,62
FITEM,2,-71
FITEM,2,74
FITEM,2,83
FITEM,2,86
FITEM,2,95
FITEM,2,98
```

```
FITEM,2,107
AESIZE,P51X,0.012,
!*
FLST,2,28,5,ORDE,16
FITEM,2,1
FITEM,2,12
FITEM,2,-13
FITEM,2,24
FITEM,2,-25
FITEM,2,36
FITEM,2,-37
FITEM,2,48
FITEM,2,-61
FITEM,2,72
FITEM,2,-73
FITEM,2,84
FITEM,2,-85
FITEM,2,96
FITEM,2,-97
FITEM,2,108
AESIZE,P51X,0.025,
!*
MSHAPE,0,2D
MSHKEY,1
!*
FLST,5,108,5,ORDE,2
FITEM,5,1
FITEM,5,-108
CM,_Y,AREA
ASEL, , , ,P51X
CM,_Y1,AREA
CHKMSH,'AREA'
CMSEL,S,_Y
!*
AMESH,_Y1
!*
CMDELE,_Y
CMDELE,_Y1
CMDELE,_Y2
!*
!**********(for more meshing density (see below)
FLST,5,2016,2,ORDE,2
FITEM,5,1
FITEM,5,-2016
CM,_Y,ELEM
ESEL, , , ,P51X
```

```
CM,_Y1,ELEM
CMSEL,S,_Y
CMDELE,_Y
!*!*
EREF,_Y1, , ,1,0,1,1
CMDELE,_Y1
!*
!**********************(Create & mesh meshing the Rigid Body)
K, ,-0.025,.01705,0,
K, ,-0.025,0.07756,0,
K, ,0,0.07756,0,
K, ,0.025,0.07756,0,
K, ,0.025,0.01705,0,
K, ,0.00635,0.01705,0,
K, ,0,0.01705,0,
K, ,-0.00635,0.01705,0,
K, ,-0.00635,0.00705,0,
K, ,0,.00705,0,
K, ,.00635,0.00705,0
/VIEW,1,,,1
/ANG,1
/REP,FAST
BLC4,-.00635,.00705,.00635,.01
FLST,2,1,5,ORDE,1
FITEM,2,109
FLST,8,2,3
FITEM,8,142
FITEM,8,139
VROTAT,P51X, , , , , ,P51X, ,360, ,
!*
BLC4,-.025,.01705,.025,.06051
FLST,2,1,5,ORDE,1
FITEM,2,125
FLST,8,2,3
FITEM,8,139
FITEM,8,135
VROTAT,P51X, , , , , ,P51X, ,360, ,
!*
SPH4,0,.00705,.00635
FLST,2,9,6,ORDE,2
FITEM,2,1
FITEM,2,-9
VADD,P51X
SAVE
!*
TYPE,   2
```

```
MAT,       2
REAL,      1
ESYS,      0
SECNUM,
!*
MSHAPE,1,3D
MSHKEY,0
!*
CM,_Y,VOLU
VSEL, , , ,      10
CM,_Y1,VOLU
CHKMSH,'VOLU'
CMSEL,S,_Y
!*
VMESH,_Y1
!*
CMDELE,_Y
CMDELE,_Y1
CMDELE,_Y2
!*
SAVE
!*
/UI,MESH,OFF
!*
!************************(create cylinder & sphere components)
ESEL,S,MAT,,1
NSLE,S
CM,Cylinder,NODE
NPLOT
ALLSEL,ALL
ESEL,S,MAT,,2
NSLE,S
CM,Indenter,NODE
NPLOT
ALLSEL,ALL
!*
EDCGEN,ASTS,INDENTER,CYLINDER,0,0,0,0,0, , , , ,0,10000000
SAVE
FINISH
/SOL
!*
EDVE,VELO,INDENTER,0,-1.6,0,0,0,0, , , , , ,
*DIM,time,ARRAY,2,1,1, , ,
*SET,TIME(2,1,1) , 1
*DIM,accg,ARRAY,2,1,1, , ,
*SET,ACCG(1,1,1) , 9.81
```

```
*SET,ACCG(2,1,1) , 9.81
!* Apply acceleration to the ball
EDLOAD,ADD,ACLY,0,INDENTER,TIME,ACCG, 0, , , , ,
TIME,0.02,
!* Solution Output Control
EDOPT,ADD,blank,BOTH !Output for both Ansys+Ls-Dyna
EDRST,200,
EDHTIME,200,
EDDUMP,1,
EDOUT,ALL   !Write all output files
EDHIST,CYLINDER   !for Cylinder
EDINT,8,0,    !No. of integration points for which results will be stored
EDENERGY,1,1,1,1
!*Define constraints
NPLOT
/VIEW,1,1,2,3
/ANG,1
/REP,FAST
FLST,2,16,1,ORDE,16
FITEM,2,427
FITEM,2,431
FITEM,2,516
FITEM,2,523
FITEM,2,1160
FITEM,2,-1161
FITEM,2,1223
FITEM,2,1228
FITEM,2,1912
FITEM,2,1915
FITEM,2,2009
FITEM,2,2012
FITEM,2,3097
FITEM,2,3100
FITEM,2,3191
FITEM,2,3194
!*
/GO
D,P51X, , , , , ,ALL, , , , ,
!*
/STATUS,SOLU
SOLVE
FINISH
!*************************************************
/POST1
SET,FIRST
FINISH
```

```
/POST26
FILE,'1','rst','.'
/UI,COLL,1
NUMVAR,200
SOLU,191,NCMIT
STORE,MERGE
FILLDATA,191,,,,1,1
REALVAR,191,191
file,1,his
EDREAD,2,RCFORC, , , ,
!*********************************END*********************************!
```

NOMENCLATURE

V_f	Final velocity
G	Acceleration due to gravity
H	Height
σ_1	Axial stress
σ_2	In-plane stress
σ_3	Out-of-plane stress
τ_{12}	Shear stress components acting in 1-2 plane
τ_{23}	Shear stress components acting in 2-3 plane
τ_{31}	Shear stress components acting in 3-1 plane
E_a	Longitudinal modulus
E_t	Transverse modulus
G_{12}	In-plane shear modulus
G_{23}	Out-of-plane shear modulus
ν_{12}	In-plane Poisson's ratio
ν_{23}	Out-of-plane Poisson's ratio
ρ	Density
S_1^t	Longitudinal tensile strength
S_2^t	Transverse tensile strength
S_1^c	Longitudinal compressive strength

S_2^c	Transverse compressive strength
S_{12}	In-plane shear strength
S_{23}	Ply transverse shear strength
S_1^{RC}	Residual strength
S	Scale factor for the delamination area
E_i	Steel Young Modulus
ν_i	Steel Poisson's ratio
t	Time

REFERENCES

[1] Naik, M. K., Al-Sulaiman F., Khan Z., Merah N., Mehdi M., Low Velocity Impact Behaviour of Composite Pipes. 2nd International Conference on: Applications of Traditional and High Performance Materials in Harsh Environments, AUS, (2006), ISBN 9948-42704-1.

[2] Khan Z., Merah N., K. Mezghani, Al-Sulaiman F., Environmental Degradation and its Effect on Long-Term Performance and Durability of Glass Fiber Reinforced Composite Used in Oil Production/Transportation pipes. Final report, project # ME2236, (2010).

[3] Frederick T. Wallenberger, James C. Watson, Hong Li, Glass Fibers ASM Handbook.

[4] O.I. Okoli, A. Abdul-Latif, Failure in composite laminates: overview of an attempt at prediction. Composites: Part A 33 (2002) 315–321.

[5] C.F. Li, N. Hu, Y.J. Yin, H. Sekine, H. Fukunaga, Low-velocity impact-induced damage of continuous fiber-reinforced composite laminates. Part I. An FEM numerical model. Composites: Part A 33 (2002) 1055-1062.

[6] C.F. Li, N. Hu, J.G. Cheng, H. Fukunaga, H. Sekine, Low-velocity impact-induced damage of continuous fiber-reinforced composite laminates. Part II. Verification and numerical investigation. Composites: Part A 33 (2002) 1063-1072.

[7] A.F. Johnson, A.K. Pickett, P. Rozycki, Computational methods for predicting impact damage in composite structures. Composites Science and Technology 61 (2001) 2183–2192.

[8] K.L. Alderson, K.E. Evans, Low velocity transverse impact of filament-wound pipes: Part 1. Damage due to static and impact loads. Composite Structures, 20 (1992) 37-45.

[9] P.B. Gning, M. Tarfaoui, F. Collombet, L. Riou, P. Davies, Damage development in thick composite tubes under internal loading and influence on implosion pressure: experimental observations. Composites: Part B, 36 (2005) 306-318.

[10] L.A. Ruhala, R.S. Engel, A Study of the impact performance of fiber reinforced composite laminated plates due to various relative fiber contents and densities. Journal of Thermoplastic Composite Materilas 12 (1999) 227-239.

[11] Giovanni Belingardi, Roberto Vadori, Low velocity impacts tests of laminate glass-fiber-epoxy matrix composite material plates. International Journal of Impact Engineering, 27 (2002) 213-229.

[12] David J. Elder, Rodney S. Thomson, Minh Q. Nguyen & Murray L. Scott, Review of delamination predictive methods for low speed impact of composite laminates. Composite Structures 66 (2004) 677-683.

[13] N.K. Naik, Sailendra Meduri, Polymer-matrix composites subjected to low-velocity impact: effect of laminate configuration. Composite Science and Technology 61 (2001) 1429-1436.

[14] P.B. Gning, M. Tarfaoui, F. Collombet, P. Davies, Prediction of damage in composite cylinders after impact. Journal of Composites Materials, 39 (2005) 917-928.

[15] Z. Aslan, R. Karakuzu, B. Okutan, The response of laminated composite plates under low-velocity impact loading. Composite Structures, 59 (2003) 119-127.

[16] Chian-Fong Yen, Thomas Cassin, Joel Patterson, Matt Triplett, Progressive Failure Analysis of Thin Walled Composite Tubes Under Low Energy Impact. Structures, Structural Dynamics & Materials Conference, (1998) 363-371.

[17] Seung Jo Kim, Nam Seo Goo, Tae Won Kim, The Effect of Curvature on The Dynamic Response and Impact-induced Damage in Composite Laminates. Composite Science and Technology 57 (1997) 763-773.

[18] Guiping Zhao, C.C., On Impact Damage of Composite Shells by a Low-Velocity Projectile. Journal of COMPOSITE MATERIALS, Vol. 38, No. 14, 2004, pp. 1231-1253.

[19] Ramin Hosseinzadeh, Mahmood Shokrieh, Larry Lessard, Damage behavior of fiber reinforced composite plates subjected to drop weight impacts. Composites Science and Technology 66 (2006) 61–68.

[20] Shiuh-Chuan Her, Yu-Cheng Liang, The finite element analysis of composite laminates and shell structures subjected to low velocity impact. Composite Structures 66 (2004) 277–285.

[21] ASTM (1999), ASTM D2444-99, Standard Test Method for Determination of the Impact Resistance of Thermoplastic Pipes and Fittings by Means of a Tup (Falling Weight). April 10, 1999.

[22] ASTM (2010), ASTM D2290-08, Standard Test Method for Apparent Hoop Tensile Strength of Plastic or Reinforced Plastic Pipe by Split Disk Method. March 17, 2010.

[23] Release 11.0 Documentation for ANSYS, © 2007 ANSYS Inc.

[24] Erdogan Madenci, Ibrahim Guven, The Finite Element Method and Applications in Engineering Using Ansys. The University of Arizona (2006).

[25] Ramazan Karakuzu, Emre Erbil, Mehmet Aktas, Damage prediction in glass/epoxy laminates subjected to impact loading. Indian Journal of Engineering & Materials Sciences, 17 (2010) 186-198.

[26] Hyung Yun Choi, Fu-Kuo Chang, A model for predicting damage in graphite/epoxy laminated composites resulting from low-velocity point impact. Journal of Composite Materials, 26 (14) (1992) 2134-2169.

[27] Masahiro Higuchi, Yasuji Hamaguchi, Shun Suzuki, Tadaharu Adachi, Dynamic Behavior of A Circular Tube Subjected to High Impact Loading. 6th International Symposium on Advanced Science and Technology in Experimental Mechanics, 3-5 November, 2011, Osaka, Japan.

[28] Celal Evci, Mufit Gulgec, *An experimental investigation on the impact response of composite materials*. International Jounal of Impact Engineering, 43 (2012) 40-51.

VITAE

Name : Rubaian Fahed Al-Shahrani

Nationality : Saudi Citizen

Date of Birth :2/24/1978

Email : rubaian.alshahrani@gmail.com

Address : P.O.Box # 6534, Dhahran 31311, Saudi Arabia

Academic Background : (1) Pursued B.S. in Mechanical Engineering in 2002 from King Fahd University of Petroleum & Minerals, Dhahran, Saudi Arabia. (2) Pursued M.Sc. in Mechanical Engineering in 2013 from King Fahd University of Petroleum & Minerals, Dhahran, Saudi Arabia.